

DFT AND DFTB INVESTIGATIONS ON  $\alpha$ -MANGOSTIN  
DYE ADSORBED ON TITANIUM DIOXIDE ELECTRODE  
IN DSSC APPLICATION



A Thesis Submitted in Partial Fulfillment of the Requirements  
for the Degree of Master of Science in Chemistry  
Department of Chemistry  
Faculty of Science  
Chulalongkorn University  
Academic Year 2018  
Copyright of Chulalongkorn University

การศึกษาด้วยระเบียบวิธีดีเอฟทีและดีเอฟทีบีบนสีย้อมแอลฟาแมงโกสตินดูดซับบนไทเทเนียมไดออกไซด์  
ออกไซด์เล็กโพรดในการประยุกต์ใช้เซลล์แสงอาทิตย์ชนิดสีย้อมไวแสง



วิทยานิพนธ์นี้เป็นส่วนหนึ่งของการศึกษาตามหลักสูตรปริญญาวิทยาศาสตรมหาบัณฑิต  
สาขาวิชาเคมี ภาควิชาเคมี  
คณะวิทยาศาสตร์ จุฬาลงกรณ์มหาวิทยาลัย  
ปีการศึกษา 2561  
ลิขสิทธิ์ของจุฬาลงกรณ์มหาวิทยาลัย

Thesis Title DFT AND DFTB INVESTIGATIONS ON  $\alpha$ -  
MANGOSTIN DYE ADSORBED ON TITANIUM  
DIOXIDE ELECTRODE IN DSSC APPLICATION  
By Miss Kanthira Kaewsud  
Field of Study Chemistry  
Thesis Advisor Professor VITHAYA RUANGPORNVISUTI,  
Dr.rer.nat.

---

Accepted by the Faculty of Science, Chulalongkorn University in Partial  
Fulfillment of the Requirement for the Master of Science

..... Dean of the Faculty of Science  
(Professor POLKIT SANGVANICH, Ph.D.)

THESIS COMMITTEE

..... Chairman  
(Associate Professor VUDHICHAI PARASUK, Ph.D.)

..... Thesis Advisor  
(Professor VITHAYA RUANGPORNVISUTI,  
Dr.rer.nat.)

..... Examiner  
(Associate Professor VIWAT VCHIRAWONGKWIN,  
Dr.rer.nat.)

..... External Examiner  
(Associate Professor. Chinapong Kritayakornupong,  
Dr.rer.nat.)

จุฬาลงกรณ์มหาวิทยาลัย  
CHULALONGKORN UNIVERSITY

กานต์ธีรา แก้วสุด : การศึกษาดัวยระเบียบวิธีดีเอฟทีและดีเอฟทีบีบนสีย้อมแอลฟาแมงโกสตินดูดซับบนไทเทเนียมไดออกไซด์อิเล็กโทรดในการประยุกต์ใช้เซลล์แสงอาทิตย์ชนิดสีย้อมไวแสง. ( DFT AND DFTB INVESTIGATIONS ON  $\alpha$ -MANGOSTIN DYE ADSORBED ON TITANIUM DIOXIDE ELECTRODE IN DSSC APPLICATION) อ.ที่ปรึกษาหลัก : ศ. ดร.วิทยา เรืองพรวิสุทธิ

โครงสร้างของสีย้อมแอลฟาแมงโกสติน (1,3,6-Trihydroxy-7-methoxy-2,8-bis(3-methyl-2-buten-1-yl)-9H-xanthen-9-one) จำนวนสามโครงสร้าง ได้รับการศึกษาในระบบแก๊ส อะซิโตน ไนโตรล์ และน้ำ โครงสร้างโมเลกุล โครงสร้างทางอิเล็กทรอนิกส์ และยูวี-วิสิเบิลสเปกตรัมของโครงสร้างทั้งหมดในตัวกลางต่างๆ หาได้โดยวิธีดีเอฟทีและดีเอฟทีบี จากการศึกษพบว่าโครงสร้างของสีย้อมแอลฟาแมงโกสตินเป็นสารไวแสงในการประยุกต์ใช้เซลล์แสงอาทิตย์ชนิดสีย้อมไวแสง โดยประสิทธิภาพการแปลงพลังงานแสงอาทิตย์เป็นพลังงานไฟฟ้า (LHEs) ในแก๊ส มีค่าอยู่ระหว่าง 0.6757 ถึง 0.7556 อิเล็กตรอนโวลต์ ในอะซิโตนไนโตรล์ มีค่าอยู่ระหว่าง 0.8286 ถึง 0.8466 อิเล็กตรอนโวลต์ และในน้ำ มีค่าอยู่ระหว่าง 0.8288 ถึง 0.8465 อิเล็กตรอนโวลต์ นอกจากนี้ค่าแรงดันไฟฟ้าขณะเปิดวงจร (Voc) ของทั้งสามโครงสร้างมีค่าอยู่ระหว่าง 2.07 ถึง 2.14 และ 1.96 ถึง 1.97 อิเล็กตรอนโวลต์ ในแก๊สและสารละลายตามลำดับ



สาขาวิชา เคมี  
ปีการศึกษา 2561

ลายมือชื่อนิสิต .....  
ลายมือชื่อ อ.ที่ปรึกษาหลัก .....

# # 6071908223 : MAJOR CHEMISTRY

KEYWORD DFT, DFTB, DYE SENSITIZED SOLAR CELLS,  $\alpha$ -MANGOSTIN  
D: DYE, SIMULATED UV-VIS SPECTRA

Kanthira Kaewsud : DFT AND DFTB INVESTIGATIONS ON  $\alpha$ -MANGOSTIN DYE ADSORBED ON TITANIUM DIOXIDE ELECTRODE IN DSSC APPLICATION. Advisor: Prof. VITHAYA RUANGPORNVISUTI, Dr.rer.nat.

Conformations of  $\alpha$ -mangostin dye (1,3,6-Trihydroxy-7-methoxy-2,8-bis(3-methyl-2-buten-1-yl)-9H-xanthen-9-one) were studied and three conformers were found as three co-existing species in various media (in vacuo, acetonitrile and water). Geometries, electronic structures and UV-Vis spectra of all conformers in various media have been obtained using density functional theory (DFT) and time-dependent DFT (TD-DFT) methods. The conformers of  $\alpha$ -mangostin dye were inspected as photosensitizers for application in dye sensitized solar cells (DSSCs) and their light-harvesting efficiencies (LHEs) within the range of 0.6757–0.7556 eV (in vacuo), 0.8286–0.8466 eV (in acetonitrile) and 0.8288–0.8465 eV (in water) were obtained. The open circuit voltage ( $V_{oc}$ ) of three conformers within the range of 2.07 to 2.14 eV (in vacuo) and 1.96 to 1.97 eV (in solvents) which may be acceptable for DSSCs were found.



Field of Study: Chemistry

Student's Signature

Academic Year: 2018

Advisor's Signature

Year:

.....

## ACKNOWLEDGEMENTS

Firstly, I am deeply grateful to my advisor, Professor Vithaya Ruangpornvisuti for his patient guidance, enthusiastic encouragement and valuable suggestions throughout the period of study. His deep insights helped me at various stages of my research.

I am also extremely grateful to Associate Professor Vudhichai Parasuk, Associate Professor Viwat Vchirawongkwin and Associate Professor Chinapong Kritayakornpong for generously offering their time for insightful comments and suggestions of my thesis.

My sincere thanks to all members of my laboratory for their helps and friendship. Special thanks to Miss Benjawan Kaewruksa for her encouragement and good suggestions throughout my time here.

Besides, I would like to thank the Development and Promotion of Science and Technology Talents Project (DPST) for financial support and the Department of Chemistry, Faculty of Science, Chulalongkorn University for research facilities.

Finally, but by no means least, I would like to acknowledge the people who mean world to me, my mother, father and sisters. I consider myself the luckiest in the world to have such a supportive family, always believing and standing beside me with their unconditional love and support. I am very proud to be a part of my family.

จุฬาลงกรณ์มหาวิทยาลัย  
CHULALONGKORN UNIVERSITY

Kanthira Kaewsud

# TABLE OF CONTENTS

	<b>Page</b>
ABSTRACT (THAI) .....	iii
ABSTRACT (ENGLISH).....	iv
ACKNOWLEDGEMENTS.....	v
TABLE OF CONTENTS.....	vi
LIST OF TABLES.....	viii
LIST OF FIGURES .....	ix
CHAPTER I INTRODUCTION.....	1
1.1 Background.....	1
1.2 The structure and operational principle of DSSCs .....	2
1.3 Titanium dioxide.....	4
1.4 The $\alpha$ -mangostin dye.....	6
1.5 Objectives .....	7
CHAPTER II THEORETICAL BACKGROUND.....	8
2.1 Semi-empirical method .....	8
2.2 Ab initio method.....	8
2.2.1 The Hartree-Fock Method .....	9
2.2.2 Slater Determinants .....	10
2.3 Density functional theory (DFT) method .....	10
2.3.1 Kohn-Sham equations.....	11
2.3.2 Exchange-Correlation Functionals .....	12
2.3.2.1 The local-density approximation (LDA) .....	12
2.3.2.2 The generalised gradient approximation (GGA).....	13
2.4 Basis sets.....	13
2.4.1 Slater-type orbitals (STOs) .....	13
2.4.2 Gaussian Type Orbitals (GTO) .....	14

2.4.3 Minimal basis sets .....	14
2.4.4 Split valence basis sets .....	14
2.4.5 Polarized basis sets .....	14
2.4.6 Diffuse functions .....	15
2.5 The self-consistent charge density functional tight binding (SCC-DFTB) .....	15
2.6 Thermochemistry .....	17
2.7 Overall efficiencies of DSSCs .....	19
CHAPTER III COMPUTATIONAL DETAILS .....	21
3.1 The optimized structure of $\alpha$ -mangostin .....	21
3.1.1 DFT and TD/DFT methods .....	21
3.1.2 Periodic DFT method .....	21
3.1.3 DFTB method .....	22
3.2 Simulation of UV-Vis spectrum .....	22
CHAPTER IV RESULTS AND DISCUSSION .....	24
4.1 Conformation, deprotonation and dehydrogenation of $\alpha$ -mangostin .....	24
4.1.1 Conformers of the $\alpha$ -mangostin .....	24
4.1.2 Deprotonations and dehydrogenation of $\alpha$ -mangostin .....	25
4.2 The most three stable conformers of the $\alpha$ -mangostin in various media .....	32
4.2.1 Equilibrium constants of interconversion between conformers .....	33
4.2.2 Simulated UV-Vis spectra of the mixture of dye conformers .....	38
4.2.3 Simulated UV-Vis spectra of the Conformer 2 bonded on TiO <sub>2</sub> .....	45
4.3 Light harvesting efficiency and open circuit voltage .....	47
4.4 Free energy of electron injection, regeneration and recombination .....	48
CHAPTER V CONCLUSIONS .....	51
REFERENCES .....	53
VITA .....	59



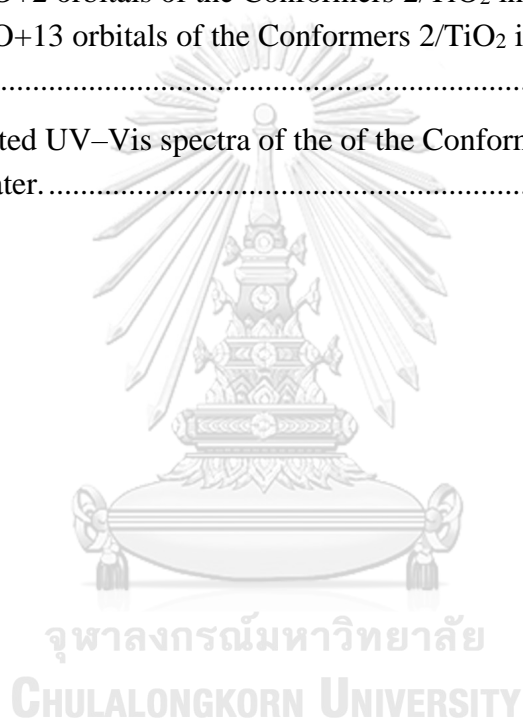
## LIST OF TABLES

	<b>Page</b>
Table 1. Structural parameters of anatase and rutile TiO <sub>2</sub> .....	6
Table 2. Energies of frontier orbitals and energy gaps of five conformers of the $\alpha$ -mangostin, their deprotonated and dehydrogenated species in various media, based on their B3LYP/6-31G+(d,p)-optimized structures.....	27
Table 3. Total energies of $\alpha$ -mangostin (LOH) conformers, their deprotonated (LO <sup>-</sup> ), dehydrogenated (LO <sup>•</sup> ) species and relative energies in gas phase, computed at various methods.....	28
Table 4. Identification based on functional group orientations of conformers.....	29
Table 5. Total energies of $\alpha$ -mangostin (LOH) conformers, their deprotonated (LO <sup>-</sup> ), dehydrogenated (LO <sup>•</sup> ) species and relative energies in various media, computed based on B3LYP/6-31+G(d,p) method.....	31
Table 6. The Gibbs free energy changes of interconversion between three major conformers and their equilibrium constants at 298 K, 1 atm, in various media.....	34
Table 7. Energetic and thermodynamics of three most stable conformers in various media and of their molecule distribution.....	35
Table 8. The reaction energy, enthalpy and Gibbs free energy changes of interconversion between three major conformers at 298 K, 1 atm, in various media.....	37
Table 9. Major transitions of three maximum wavelengths of the three most stable conformers of $\alpha$ -mangostin in various media.....	39
Table 10. The wavelength of maximum absorptivity ( $\lambda_{\max}^1$ ) and oscillator strengths (f) of the UV-Vis spectra of three most stable conformers in various media.....	40
Table 11. The open circuit voltage ( $V_{OC}$ ) and light harvesting efficiency (LHE) of three conformers of the $\alpha$ -mangostin in various media.....	48
Table 12. Values of $E_{\lambda_{\max}}$ , $E^{dye}$ and $E^{dye*}$ of three conformers of the $\alpha$ -mangostin in various media.....	49
Table 13. Terms of free energy changes of three conformers of the $\alpha$ -mangostin in various media.....	50

## LIST OF FIGURES

	Page
Figure 1. Schematic representation of DSSC device structure. ....	3
Figure 2. Crystal structures of TiO <sub>2</sub> rutile (tetragonal, space group <i>P4<sub>2</sub>/mnm</i> ), brookite (orthorhombic, space group <i>Pbca</i> ) and anatase (tetragonal, space group <i>I4<sub>1</sub>/amd</i> ) polymorphs <sup>27</sup> .....	4
Figure 3. Structure of (a) anatase (101), (b) anatase (001), (c) rutile (110) and (d) rutile (001) surfaces <sup>32</sup> .....	5
Figure 4. Chemical structure of $\alpha$ -mangostin.....	7
Figure 5. Optimized structures of five conformers of the $\alpha$ -mangostin in gas phase obtained by (a) B3LYP/6-31+G(d,p), (b) periodic DFT and (c) periodic DFTB computations. Notes: D1=C14-C1-C2-C3, D2=C1-C2-C3-C4, D3=C2-C3-C4-C5, D4=C7-C6-O2-H1, D5=C6-C7-C8-C9, D6=C7-C8-C9-C10, D7=C8-C9-C10-C11, D8=C7-C12-O3-H2, D9=C14-C13-O5-H3, D10=C13-C14-O6-C15. ....	26
Figure 6. B3LYP/6-31+G(d,p)-optimized structures of five conformers of the $\alpha$ -mangostin in (a) gas phase, (b) acetonitrile and (c) water. Notes: D1=C14-C1-C2-C3, D2=C1-C2-C3-C4, D3=C2-C3-C4-C5, D4=C7-C6-O2-H1, D5=C6-C7-C8-C9, D6=C7-C8-C9-C10, D7=C8-C9-C10-C11, D8=C7-C12-O3-H2, D9=C14-C13-O5-H3, D10=C13-C14-O6-C15.....	30
Figure 7. Electrostatic potential maps with iso-surface value of 0.03 e $\text{\AA}^{-3}$ , showing charge density distribution in three most stable conformers of the $\alpha$ -mangostin in (a) gas phase, (b) acetonitrile and (c) water, based on their B3LYP/6-31+G(d,p)-optimized structures. ....	32
Figure 8. Interconversions of three major conformers of the $\alpha$ -mangostin. Values in parentheses and square brackets are systems in acetonitrile and water, respectively otherwise in gas phase. Gibbs free energy changes are in kcal/mol and equilibrium constants are unitless.....	36
Figure 9. The orbitals related with major electron transitions according to UV-Vis spectra of the Conformers 2, 3 and 4 in gas phase (the first row), acetonitrile (the second row) and water (the third row). ....	42
Figure 10. The simulated UV/Vis absorption spectra of $\alpha$ -mangostin conformers (Conformer 2, 3 and 4) in (a) gas phase, (b) acetonitrile and (c) water, based on their corresponding TD/B3LYP/6-31+G(d,p) calculations. ....	43

- Figure 11. Simulated UV–Vis spectra of mixtures of three major conformers of the  $\alpha$ -mangostin and their components (Conformers 2, 3 and 4) in (a) gas phase, (b) acetonitrile and (c) water. ....44
- Figure 12. Most stable structures of Conformers 2/TiO<sub>2</sub> (001) surface in (a) vacuo, (b) acetonitrile and (c) water. The Conformers 2/TiO<sub>2</sub> in vacuo were optimized using the B3LYP method and in solvents using the CPCM/UFF/B3LYP method, with mixed basis sets (LanL2Dz and 6–31–G+(d,p) are for Ti and other atoms, respectively). ....45
- Figure 13. The orbitals related with major electron transitions, plotted of (a) the HOMO and LUMO+2 orbitals of the Conformers 2/TiO<sub>2</sub> in vacuo, (b) and (c) the HOMO and LUMO+13 orbitals of the Conformers 2/TiO<sub>2</sub> in acetonitrile and water, respectively. ....46
- Figure 14. Simulated UV–Vis spectra of the of the Conformers 2/TiO<sub>2</sub> in vacuo, acetonitrile and water. ....47



# CHAPTER I

## INTRODUCTION

### 1.1 Background

Nowadays, the fossil fuels are the main sources of energy used all over the world. The burning of the fossil fuels emits ton of carbon dioxide that pollute the environment and also change the climatic conditions. Consequently, the search for utilize renewable energy sources have become more important <sup>1</sup>. Dye-sensitized solar cells (DSSCs) are a type of solar cells that were evaluated as one choice of alternative technology for the conversion of solar energy into electricity <sup>2</sup>. Due to their simple fabrication, low production cost, environmental friendliness and good conversion efficiencies, this technology was in place of the conventional solar energy <sup>3-5</sup>.

The performance of the cell depends heavily on a dye used as a sensitizer <sup>6</sup>. In recent years, several of natural dyes extracting from natural materials such as flowers, leaves, fruits, traditional Chinese medicines, carrot, mulberry, purple cabbage, potato and grapes <sup>7</sup>, instead of synthetic dyes were fabricated in DSSCs <sup>8</sup>. The natural dyes have several advantages such as low cost, non-toxicity, easy to prepare and no pollution to environment <sup>8-10</sup>. The natural dye,  $\alpha$ -mangostin which is a xanthone was extracted from mangosteen (*Garcinia mangostana* Linn) peel and pericarp which is highly valuable agricultural waste <sup>11</sup>. The  $\alpha$ -mangostin is natural dye were used as photosensitizers in DSSCs <sup>12</sup>.

From the point of view, several works have focused on natural dye based DSSCs. In 2010, Zhou and co-workers reported twenty natural dyes obtained from nature, including flowers, leaves of plants, fruits, traditional Chinese medicines, and beverages, were used as sensitizers. They found that the open circuit voltages ( $V_{oc}$ ) are within the range 0.337 to 0.689 V, and the short circuit photocurrent densities ( $J_{sc}$ ) ranged from 0.14 to 2.69 mA cm<sup>-2</sup>. Interestingly, the dye extracted from mangosteen pericarp offered the highest efficiency of 1.17% compared with twenty natural dyes <sup>11</sup>. W. Maiaugree and co-workers focused on the preparation and photovoltaic

performance of natural dye based DSSC. The photosensitizer and counter electrode made from mangosteen peel and carbonized mangosteen peel film, respectively. The efficiency of the DSSC sensitized was 2.63% in which higher than that of Pt counter electrode (1.47%)<sup>6</sup>. Furthermore, S. Tontapha and co-workers studied  $\alpha$ -mangostin and anthocyanin extracted from mangosteen pericarp as sensitizers for DSSCs. The maximum efficiencies ( $\eta$ ) of 1.78 and 1.63% for  $\alpha$ -mangostin sensitization were obtained in acidified acetone and ethanol, respectively<sup>12</sup>.

## 1.2 The structure and operational principle of DSSCs

Dye-sensitized solar cells (DSSCs) are a third generation of solar cell invented by O'Regan and Gratzel in 1991<sup>13</sup>. DSSCs typically consist of four main parts which are working electrode, counter electrode, dye-sensitizer and redox electrolyte<sup>14</sup>. All of which are sandwiched together between two electrodes and the electrolyte, typically containing the iodide/triiodide ( $I^-/I_3^-$ ) redox, fills the gap between them<sup>15-16</sup>. The working electrode is covered with a film of small dye-sensitized semiconductor particles while the counter electrode is coated with a catalyst<sup>17-18</sup>.

In DSSCs, light is harvested by dye molecules grafted on the surface of semiconductor. As a result, the electron from the ground state is transferred to excited state and then injected from the lowest unoccupied molecular orbital (LUMO) of the dye into the conduction band of  $TiO_2$  semiconductor. The dye that lose electrons can be recovered to its original state by the donation of electrons from the electrolyte such as  $I_3^-/I^-$ . Then, the iodide is regenerated in turn by the reduction of triiodide at the counter electrode. Therefore, the dye and electrolyte solution regain original state<sup>19-22</sup>. The schematic diagram of DSSC can be seen in Figure 1.

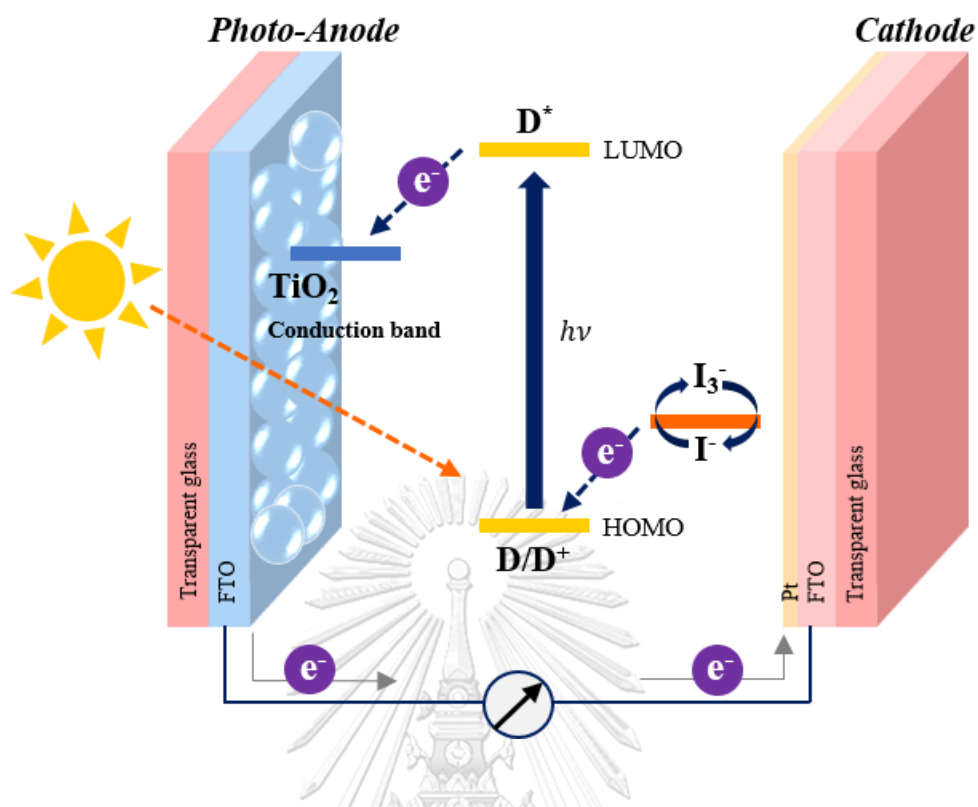


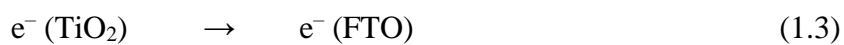
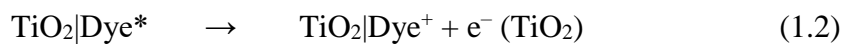
**Figure 1.** Schematic representation of DSSC device structure.

In brief, the basic sequence of events in a DSSC is as follows <sup>23</sup>.

Activation



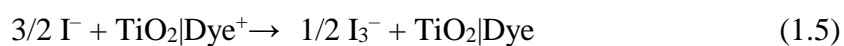
Electron injection



Electron reception



Interception reaction



### 1.3 Titanium dioxide

Titanium dioxide ( $\text{TiO}_2$ ) is widely used as photoanode in DSSCs due to its suitable valence band and conduction band positions, long-term stability, non-toxicity, and cost-effectiveness<sup>24-25</sup>. The morphology, porous structure and crystallinity of  $\text{TiO}_2$  play critical roles in the photoelectric conversion efficiency of DSSCs. In nature,  $\text{TiO}_2$  occurs as three polymorphs namely rutile, anatase and brookite<sup>26</sup> as presented in Figure 2.

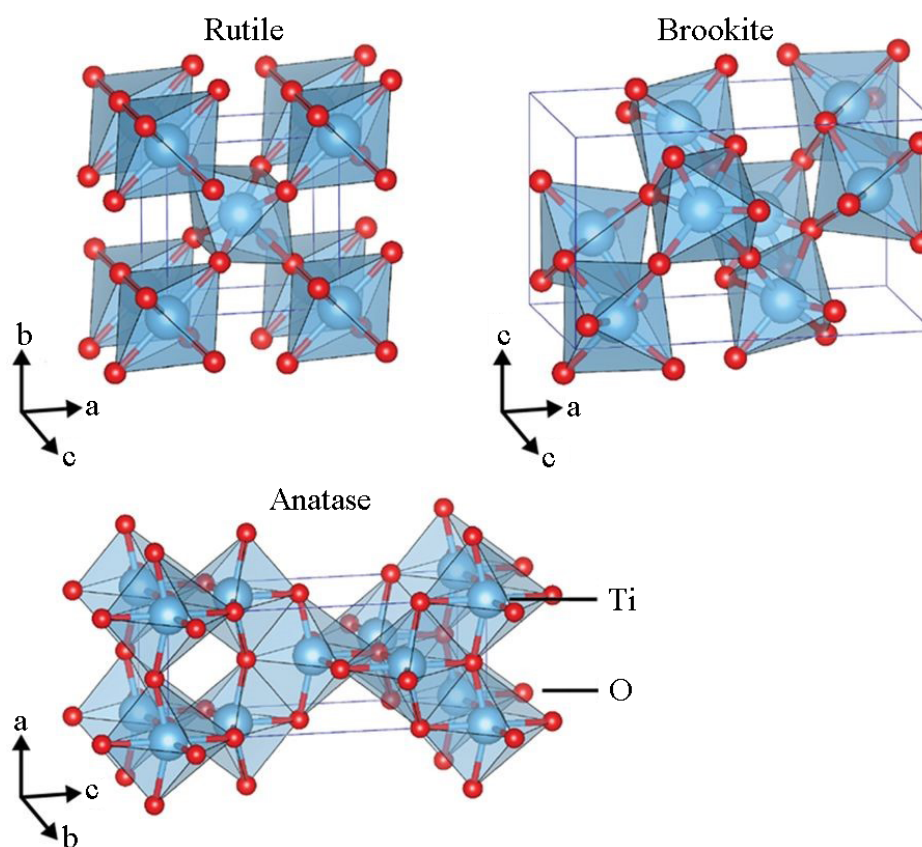


**Figure 2.** Crystal structures of  $\text{TiO}_2$  rutile (tetragonal, space group  $P4_2/mnm$ ), brookite (orthorhombic, space group  $Pbca$ ) and anatase (tetragonal, space group  $I4_1/amd$ ) polymorphs<sup>27</sup>.

In all three structures, the basic building block consists of a titanium atom surrounded by six oxygen atoms in a distorted octahedral<sup>28</sup>. The oxidation state of Ti and O are formally +4 and -2, respectively. Rutile and anatase have a tetragonal geometry, differently from brookite which has an orthorhombic geometry<sup>29</sup>. Rutile is the most thermodynamically stable phase, whereas anatase and brookite phase are metastable and unstable<sup>30</sup>. In rutile structure each octahedron is in contact with ten neighbor octahedrons (two sharing edge oxygen pairs and eight sharing corner oxygen atoms) while in anatase structure each octahedron is in contact with eight neighbor octahedrons (four sharing an edge and four sharing a corner)<sup>31</sup>.

The structures of the rutile (001), (101) and anatase (001), (110) surfaces are showed in Figure 3. Rutile has a body-centered tetragonal unit cell with cell parameters of  $a=b=0.4594$  nm and  $c=0.2959$  nm as illustrated in Table 1. All the Ti atoms are fourfold coordinated and all the O atoms twofold coordinated.

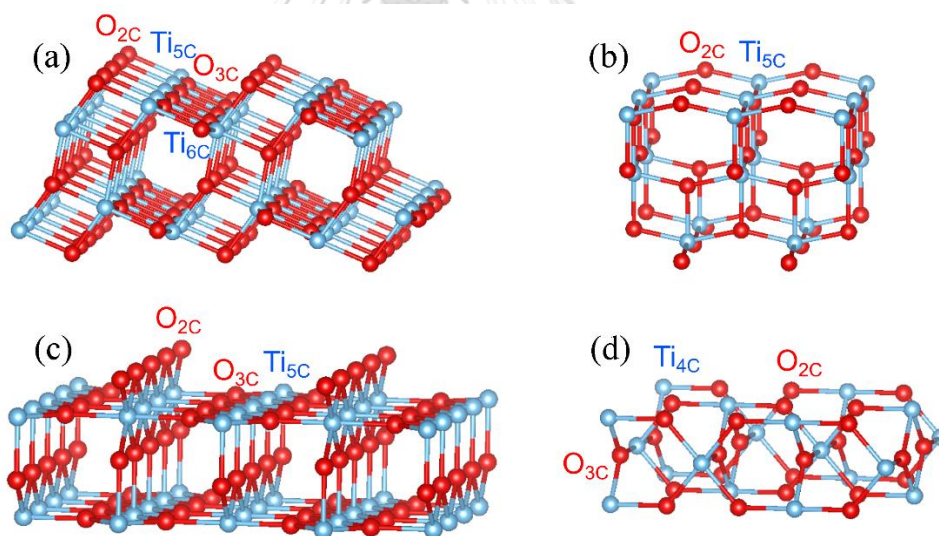


**Figure 3.** Structure of (a) anatase (101), (b) anatase (001), (c) rutile (110) and (d) rutile (001) surfaces<sup>32</sup>.



**Table 1.** Structural parameters of anatase and rutile TiO<sub>2</sub>.

	Anatase	Rutile
Bravias lattice	Body-centered tetragonal	Primitive tetragonal
Space group	No. 141 <i>I</i> 4 <sub>1</sub> /amd	No. 136 <i>P</i> 4 <sub>2</sub> /mmm
Lattice parameters [Å] <sup>a</sup>		
a	3.785	4.594
b	3.785	4.594
c	9.514	2.959
Band gap energy [eV]	3.2 <sup>b</sup>	3.0 <sup>c</sup>
Density [g/cm <sup>3</sup> ] <sup>d</sup>	3.894	4.250

<sup>a</sup> Ref. <sup>33</sup>

<sup>b</sup> Ref. <sup>34</sup>

<sup>c</sup> Ref. <sup>35</sup>

<sup>d</sup> Ref. <sup>36</sup>

#### 1.4 The $\alpha$ -mangostin dye

Mangosteen (*Garcinia mangostana* Linn) is a tropical fruit that mainly found in Southeast Asian countries such as Malaysia, Myanmar, Thailand, Philippines, Sri Lanka and India. It is known as the queen of fruits in Thailand because of its unique taste and flavor. The main components in the mangosteen peel extract were  $\alpha$ -mangostin which is a yellowish coloring matter. The compound can be obtained from the other parts of the plant such as the dried sap and the bark. The  $\alpha$ -mangostin was found to have anti-inflammatory <sup>37-40</sup>, antibacterial <sup>41-42</sup>, anti-tumor <sup>43</sup> properties and anti-metastatic properties in many cancer cell types <sup>44</sup>. Biological activities and pharmacological properties of  $\alpha$ -mangostin as an antineoplastic agent, antioxidant, anti-proliferation and induces apoptosis were reviewed <sup>45</sup>. Antioxidant and neuroprotective effects of the  $\alpha$ -mangostin on 6-hydroxydopamine-induced toxicity in SH-SY5Y cells as an in vitro model for Parkinson's disease were demonstrated <sup>46</sup>. Besides, the  $\alpha$ -mangostin was found to inhibit both dengue virus production and

cytokine/chemokine<sup>47</sup>. The three hydroxyl (–OH) groups are found in the structure as shown in Figure 4. Therefore, a possible anchoring mode is monodentate coordination via its available hydroxyl group.

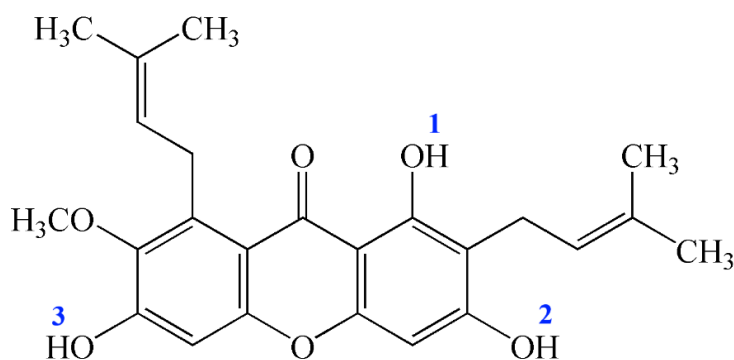


**Figure 4.** Chemical structure of  $\alpha$ -mangostin.

### 1.5 Objectives

In this work, we have investigated the conformations of  $\alpha$ -mangostin dye using DFT, periodic DFT and DFTB methods. Structures of deprotonated, dehydrogenated species of all conformers and related reactions in vacuo, acetonitrile and water have been obtained to comprehend and predict their interactions with other substrates and semiconducting materials as electrodes. Thermodynamic properties of all existing species have been evaluated and equilibrium constants of interconversion of co-existing conformers have been derived from their related Gibbs free energy changes in vacuo, acetonitrile and water. The simulated UV–Vis spectra of each conformer in different media have been constructed using TD–DFT and Gaussian distribution functional methods. The light harvesting efficiency (*LHE*), open circuit voltage ( $V_{OC}$ ) and relative terms of dye sensitized solar cells (DSSCs) performance of  $\alpha$ -mangostin dye on  $TiO_2$  with  $I_3^-/I^-$  redox electrolyte of various media have been reported.

## CHAPTER II

### THEORETICAL BACKGROUND

Computational chemistry is one of the most fascinating branches of chemistry that is widely used to investigate the molecular structures, molecular properties, reactions mechanisms and energetics. There are two types of computational chemistry namely quantum mechanics (QM) and molecular mechanics (MM). Quantum mechanical method is categorized into semi-empirical, ab initio and density functional theory (DFT) methods.

#### 2.1 Semi-empirical method

Semi-empirical methods are based on the principle of quantum chemistry which derived from Hartree-Fock calculations by applying empirical corrections. The integrals are determined directly from experimental data. The advantage of semi-empirical calculations is reduced computation time, making them commonly used in the application for large molecules<sup>48</sup>. The methods in semi-empirical such as PM3, AM1 and MNDO are generally used for predicting various properties such as molecular structure, heats of formation, ionization potentials and electron affinities<sup>49</sup>.

#### 2.2 Ab initio method

Ab initio methods involve quantum mechanical calculations which are derived directly from theoretical principles without appeal to fitting to experiment. The simplest type of ab initio calculation is Hartree-Fock method. These calculations take much longer than semi-empirical methods because the Coulombic electron-electron repulsion is taken into consideration by integrating the repulsion term<sup>50</sup>.

### 2.2.1 The Hartree–Fock Method

The Hartree–Fock method is a single electron approximation technique used in many–particle system. The molecular Hamiltonian is split up into individual single electron Hamiltonians. Each molecular orbital is expressed as a linear combination of atomic orbitals. The plausible approximate polyelectronic wavefunction can be described as the product of one–electron wavefunctions <sup>51</sup>.

$$\Psi_0 = \psi_0(1)\psi_0(2)\psi_0(3)\cdots\psi_0(n) \quad (2.1)$$

where  $\Psi_0$  is a function of the coordinates of all electrons in the atoms,  $\psi_0(1)$  is a function of the coordinates of electron 1 and  $\psi_0(2)$  is a function of the coordinates of electron 2.

To solve one–electron Schrödinger equation, the only moving particle in Eq (2.1) is electron one. To solve for electron 2, a one–electron Schrödinger equation with electron two moving in an average field due to the electrons of continuing to electron moving in a field due to the electrons of  $\psi_1(1), \psi_1(3), \dots, \psi_1(n)$ , continuing to electron  $n$  moving in a field due to  $\psi_1(1), \psi_1(2), \dots, \psi_1(n-1)$ . The first cycle of calculations can be expressed as

$$\Psi_1 = \psi_1(1)\psi_1(2)\psi_1(3)\cdots\psi_1(n) \quad (2.2)$$

Repetition of the cycle gives

$$\Psi_2 = \psi_2(1)\psi_2(2)\psi_2(3)\cdots\psi_2(n) \quad (2.3)$$

The process is continued for  $k$  cycles until obtained a wavefunction  $\psi_k$  and energy calculated from  $\psi_k$ .

### 2.2.2 Slater Determinants

One way of constructing such a wave function is the so-called Hartree product defined as the product of all the one-electron wave functions of the system.

$$\Psi(x) = \psi_1(x_1)\psi_2(x_2)\cdots\psi_N(x_N) \quad (2.4)$$

However, this approach of defining the many-electron wave function is not valid for electrons due to the Pauli exclusion principle which the wave function of electrons should be antisymmetric. Nevertheless, the one-electron wave functions in Eq (2.4) can create an antisymmetrical many-electron wave function. This permutation is then called the Slater determinant as expressed in Eq (2.5).

$$\Psi(x) = |\psi_1\psi_2\cdots\psi_N| = \frac{1}{\sqrt{N!}} \begin{vmatrix} \psi_1(x_1) & \psi_1(x_2) & \cdots & \psi_1(x_N) \\ \psi_2(x_1) & \psi_2(x_2) & \cdots & \psi_2(x_N) \\ \vdots & \vdots & \ddots & \vdots \\ \psi_N(x_1) & \psi_N(x_2) & \cdots & \psi_N(x_N) \end{vmatrix} \quad (2.5)$$

### 2.3 Density functional theory (DFT) method

Density functional theory (DFT) within the orbital formulation by Kohn–Sham (KS) is a very powerful method to investigate the physical and chemical properties of molecules. The energy of a system is calculated as a function of the electron density, not as a function of the coordinates of each electron. It is a very successful complement to the wave function-based methods, which build upon Hartree–Fock (HF) theory to include electron correlation.

### 2.3.1 Kohn–Sham equations

The Kohn–Sham equations for one–electron Schrödinger–like equation can be written as <sup>52</sup>

$$\left( -\frac{1}{2}\nabla^2 + \nu(r) + \int \frac{\rho(r')}{|r-r'|} dr' + \nu_{xc}(r) \right) \phi_i = \varepsilon \phi_i \quad (2.6)$$

where  $\phi$  is the Kohn–Sham orbitals,  $\varepsilon$  is the energy of the Kohn–Sham orbital,  $\nu_{xc}$  is the exchange–correlation potential and  $\rho(r)$  is the electron density.

The electron density is obtained as

$$\rho(r) = \sum_i^N |\phi_i|^2 \quad (2.7)$$

In addition, the exchange–correlation potential is given by

$$\nu_{xc}(r) = \frac{\delta E_{xc}[\rho]}{\delta n(r)} \quad (2.8)$$

where  $E_{xc}[\rho]$  is the exchange–correlation functional. The effective potential ( $\nu_{eff}$ ) is defined by

$$\nu_{eff} = \nu(r) + \int \frac{\rho(r')}{|r-r'|} dr' + \nu_{xc}(r) \quad (2.9)$$

This allows Eq (2.6) to be rewritten as <sup>53</sup>

$$\left( -\frac{1}{2}\nabla^2 + \nu_{eff} \right) \phi_i = \varepsilon \phi_i \quad (2.10)$$

Finally, the total energy of the system is defined as

$$E = \sum_i^N \varepsilon_i - \frac{1}{2} \iint \frac{\rho(r)\rho(r')}{|r-r'|} drdr' + E_{xc}[\rho] - \int \nu_{xc}(r)\rho(r)dr \quad (2.11)$$

### 2.3.2 Exchange–Correlation Functionals

The exchange–correlation ( $E_{xc}[\rho]$ ) energy can be classified into the local–density approximation (LDA) and the generalized gradient approximation (GGA) <sup>54</sup>.

#### 2.3.2.1 The local–density approximation (LDA)

The local density approximation (LDA) in density functional theory (DFT) can be used by writing the exchange–correlation energy as a sum of exchange and correlation part. The total exchange–correlation energy can be written as

$$E_{xc}^{LDA}[n] = \int n(r)\varepsilon_{xc}^{unif}(n(r))dr \quad (2.12)$$

where  $\varepsilon_{xc}^{unif}$  is the exchange–correlation energy per particle of the interacting uniform electron gas of density  $n(r)$ . The exchange energy can be expressed as

$$E_{xc}^{LDA}[n] = -\frac{3}{4} \left( \frac{3}{\pi} \right)^{1/3} \int n^{4/3}(r)dr \quad (2.13)$$

### 2.3.2.2 The generalised gradient approximation (GGA)

A more generally used exchange–energy functional based on the generalized–gradient approximation (GGA) is given by

$$E_{XC}^{GGA} = \int n(r) \varepsilon_{XC}^{unif}(n(r)) F_X^{GGA}(s) dr \quad (2.14)$$

where  $F_X^{GGA}(s)$  is the exchange enhancement factor.

## 2.4 Basis sets

A basis set in computational chemistry is a set of functions which are linear combinations with atomic orbitals used to create the molecular orbitals<sup>55</sup>. The common basis functions in quantum chemistry consists of two types namely Slater–type orbitals (STO) and Gaussian type orbitals (GTO)<sup>56</sup>.

### 2.4.1 Slater–type orbitals (STOs)

Slater–type orbitals (STO) are the natural basis functions in quantum molecular calculations used as atomic orbitals. The STO's have the form

$$f^{STO} = \left( \frac{\zeta}{\pi} \right)^{\frac{1}{2}} \exp -\zeta r \quad (2.15)$$

where  $\zeta$  denotes the Slater orbital exponent,  $r$  is radius in angstroms. However, it is very difficult to evaluate the more two atoms due to mathematical integration. Thus, a popular alternative to STOs is the Gaussian type orbitals (GTO)<sup>57</sup>.



### 2.4.2 Gaussian Type Orbitals (GTO)

The Gaussian type orbitals (GTO) or Gaussian type functions (GTF) are alternative functions to the STOs in the molecular calculations. These functions were first proposed by Boys and McWeeny in 1950. And it can be expressed as followed <sup>58</sup>

$$f^{GTO} = \left( \frac{2\alpha}{\pi} \right)^{\frac{3}{4}} \exp -\alpha r^2 \quad (2.16)$$

### 2.4.3 Minimal basis sets

Minimal basis sets are the simplest type of basis set. It contains the minimum number of basis functions that are required to describe the occupied atomic orbitals of each atom <sup>59</sup>. There are two types of minimal basis sets that are Slater-type orbitals (STO) and Gaussian type orbitals (GTO). The most general is STO-nG, where n is represents the number of Gaussian primitive functions comprising a single basis function. The most general used are STO-3G, STO-4G and STO-6G <sup>60</sup>.

### 2.4.4 Split valence basis sets

The split-valence basis sets are treated only one basis function for the core electrons while the valence electrons can be treated with a larger basis set. Two basis functions are used for each valence atomic orbital as an inner-shell and outer-shell. The general split-valence basis sets are 3-21G, 4-31G, and 6-31G <sup>56, 61</sup>.

### 2.4.5 Polarized basis sets

Polarization functions are represented after the G, with a separate designation for non-hydrogen atoms and hydrogen. These basis sets are denoted by one asterisk (\*) or two asterisks (\*\*), with one asterisk means that polarization has been taken into the heavy atoms while two asterisks (\*\*) indicates that polarization functions are added to hydrogen <sup>62-63</sup>.

### 2.4.6 Diffuse functions

Diffuse functions are function with a large-size version of  $s$ - and  $p$ -type functions. Basis sets with these functions are important for systems that electrons are far from the nucleus such as molecules with lone pairs, anions and negative charges. The 6-31+G(d,p) is the 6-31G(d,p) basis set with diffuse functions added to heavy atoms<sup>64</sup>.

### 2.5 The self-consistent charge density functional tight binding (SCC-DFTB)

The DFTB method is based on a second-order expansion of the Kohn-Sham total energy in Density-Functional Theory (DFT) with respect to charge density fluctuations. The DFTB method has been applied to study large molecules, clusters, nanostructures and condensed-matter systems with a wide range of elements<sup>65</sup>.

The SCC-DFTB which includes charge self-consistency is derived from DFT by choosing a reference density  $\rho_0$  as a superposition of neutral atomic densities  $\rho_0^\alpha$   $\rho_0 = \sum_{\alpha} \rho_0^\alpha$  and expanding the DFT exchange-correlation energy functional up to the second order to obtain<sup>66</sup>

$$E = \sum_i^{occ} \langle \Psi_i | \hat{H}_0 | \Psi_i \rangle - \frac{1}{2} \iint \frac{\rho_0 \rho_0'}{|\vec{r} - \vec{r}'|} d\vec{r}' + E_{xc}[\rho_0] - \int V_{xc}[\rho_0] \rho_0 + E_{ii} + \frac{1}{2} \iint \left( \frac{1}{|\vec{r} - \vec{r}'|} + \left. \frac{\delta^2 E_{xc}}{\delta \rho \delta \rho'} \right|_{\rho_0} \right) \delta \rho \delta \rho' d\vec{r}' \quad (2.17)$$

$\delta \rho$  is the superposition of atom-like contributions ( $\delta \rho_\alpha$ ) which is written as

$$\delta \rho = \sum_{\alpha}^N \delta \rho_{\alpha} \quad (2.18)$$

where the atom-like contributions can be expressed as

$$\delta\rho_\alpha \approx \Delta q_\alpha F_{00}^\alpha Y_{00} \quad (2.19)$$

where  $\Delta q_\alpha$  ( $\Delta q_\alpha = q_\alpha - q_\alpha^0$ ) is the Mulliken charge which is the difference between the atomic Mulliken population  $q_\alpha$  and the number of valence electrons of the neutral free atom  $q_\alpha^0$ ,  $F_{00}^\alpha$  denotes the normalized radial dependence of the density fluctuation in atom  $\alpha$  approximated to spherical by the angular function  $Y_{00}$ .

$$E_{2nd} \approx \frac{1}{2} \sum_{\alpha,\beta}^N \Delta q_\alpha \Delta q_\beta \iint \left( \frac{1}{|\vec{r} - \vec{r}'|} + \left. \frac{\delta^2 E_{XC}}{\delta\rho\delta\rho'} \right|_{\rho_0} \right) F_{00}^\alpha F_{00}^\beta Y_{00}^2 d\vec{r} d\vec{r}' \quad (2.20)$$

In case of the interatomic separation is very large, the exchange–correlation term goes to zero and  $\gamma_{\alpha,\beta}$  basically reducing to  $1/|\vec{R}_\alpha - \vec{R}_\beta|$ .

$$E_{2nd} \approx \frac{1}{2} \sum_{\alpha,\beta}^N \frac{\Delta q_\alpha \Delta q_\beta}{|\vec{R}_\alpha - \vec{R}_\beta|} \quad (2.21)$$

where  $\gamma_{\alpha,\beta} = \gamma_{\alpha,\beta}(U_\alpha, U_\beta, R_{\alpha\beta})$  and  $U_\alpha = \frac{1}{2} \frac{\partial^2 E_{at}}{\partial q_{at}^2}$  is the second derivative of the energy of the atom  $\alpha$  with respect to its total charge.

$$\hat{H}_{\mu\nu}^0 = \langle \phi_\mu | \hat{H}(\rho_0) | \phi_\nu \rangle \quad (2.22)$$

$$\hat{H}_{\mu\nu} = \hat{H}_{\mu\nu}^0 + \frac{1}{2} S_{\mu\nu} \sum_\gamma \Delta q_\gamma (\gamma_{\alpha\gamma} + \gamma_{\beta\gamma}) \quad (2.23)$$

Then,  $E_{rep}$  is defined as

$$E_{rep} = -\frac{1}{2} \iint \frac{\rho'_0 \rho_0}{|\vec{r} - \vec{r}'|} + E_{XC}[\rho_0] - \int V_{XC}[\rho_0] n_0 + E_{ii} \quad (2.24)$$

$$E_{rep} = \sum_{\alpha\beta} U_{\alpha\beta} \quad (2.25)$$

Finally, the approximate DFTB total energy reads as

$$E_{tot} = \sum_{i\mu\nu} c_\mu^i c_\nu^i H_{\mu\nu}^0 + \frac{1}{2} \sum_{\alpha\beta} \Delta q_\alpha \Delta q_\beta \gamma_{\alpha\beta}(R_{\alpha\beta}) + E_{rep} \quad (2.26)$$

## 2.6 Thermochemistry

Thermochemistry is the study of the measurement and interpretation of heat changes accompanying chemical and physical processes. The enthalpies ( $\Delta_r H^\circ(298K)$ ) of reaction at 298 K can be written as:

$$\Delta_r H^\circ(298K) = \sum_{products} \Delta_f H_{products}^\circ X_i(298K) - \sum_{reactants} \Delta_f H_{reactants}^\circ(298K) \quad (2.27)$$

The Gibbs free energy ( $\Delta_f G^\circ(298K)$ ) of reaction at 298 K can be expressed as followed:

$$\Delta_f G^\circ(298K) = \Delta_f H^\circ(298K) - T(S^\circ(M, 298K)) - \sum S^\circ(x, 298K) \quad (2.28)$$

where  $M$  stand for the molecule,  $X$  represent each element which makes up  $M$ , and  $x$  will be the number of atoms of  $X$  in  $M$ .

Atomization energy of the molecule ( $\sum D_0(M)$ ) is obtained from the total energies of the molecule ( $\varepsilon_0(M)$ ), the zero-point energy of the molecule ( $\varepsilon_{ZPE}(M)$ ) and the constituent atoms as expressed below:

$$\sum D_0(M) = \sum_{atoms} x\varepsilon_0(X) - \varepsilon_0(M) - \varepsilon_{ZPE}(M) \quad (2.29)$$

Thus,  $\Delta_f H^\circ(M, 298K)$  and  $\Delta_f G^\circ(298K)$  are defined as follows

$$\begin{aligned} \Delta_f H^\circ(M, 0K) &= \sum_{atoms} x\Delta_f H^\circ(X, 0K) - \sum D_0(M) \\ &= \sum_{atoms} x\Delta_f H^\circ(X, 0K) - \left( \sum_{atoms} x\varepsilon_0(X) - \varepsilon_0(M) - \varepsilon_{ZPE}(M) \right) \end{aligned} \quad (2.30)$$

$$\begin{aligned} \Delta_f H^\circ(M, 298K) &= \Delta_f H^\circ(M, 0K) + (H_M^\circ(298K) - H_M^\circ(0K)) \\ &\quad - \sum_{atoms} x(H_X^\circ(298K) - H_X^\circ(0K)) \end{aligned} \quad (2.31)$$

$$\Delta_f G^\circ(M, 298K) = \Delta_f H^\circ(298K) - 298.15(S^\circ(M, 298K) - \sum S^\circ(X, 298K)) \quad (2.32)$$

## 2.7 Overall efficiencies of DSSCs

The performance of DSSCs is assessed in terms of the photon-to-electricity conversion efficiency (also called the power conversion efficiency of a photovoltaic device) ( $\eta$ ), which is the product of the short-circuit current ( $J_{SC}$ ), open circuit voltage ( $V_{OC}$ ) and the fill factor ( $FF$ ), divided by the incident solar power on the cell ( $P_{inc}$ )<sup>67-68</sup>, as expressed in Eq (2.33).

$$\eta = FF \cdot \frac{J_{sc} V_{oc}}{P_{inc}} \quad (2.33)$$

The  $J_{SC}$  is related to the light-harvesting efficiency ( $LHE$ )<sup>69-71</sup>, as described in Eq (2.34).

$$J_{SC} = q \int_{\lambda} LHE(\lambda) \phi_{inject} \eta_{collect} \phi(\lambda) d\lambda \quad (2.34)$$

where  $q$  is the unit of charge,  $\phi_{inject}$  is the electron injection efficiency,  $\eta_{collect}$  is charge collection efficiency and  $\phi$  is the photon flux of solar spectrum. The LHE can be computed from the oscillator strength ( $f$ ) corresponding to the maximum absorption wavelength ( $\lambda_{max}$ ) of dye molecule<sup>72</sup>, using Eq (2.35).

$$LHE = 1 - 10^{-f} \quad (2.35)$$

The excited-state energy of dye ( $E^{dye^*}$ ) can be estimated using Eq (2.36)<sup>73-74</sup>.

$$E^{dye^*} = E_{\lambda_{max}} + E^{dye} \quad (2.36)$$

where  $E^{dye}$  is the ground-state energy of dye, estimated as the energy of dye at the HOMO- $n$  level ( $E^{dye} = HOMO - n$ ) and  $E_{\lambda_{max}}$  is the energy (in eV) of maximum

absorption wavelength ( $\lambda_{\max}$ , in m), converted by  $hc / \lambda_{\max}$  ( $h=4.135667516 \times 10^{-15}$  eV s,  $c=299.792458 \times 10^6$  ms<sup>-1</sup>). The  $V_{OC}$  of which precise value can be estimated as a difference between the LUMO energy of dye and the conduction band edge of TiO<sub>2</sub> semiconductor ( $E_{CB}^{TiO_2}$ )<sup>75</sup>, using Eq (2.37).

$$V_{OC} = E_{LUMO}^{dye} - E_{CB}^{TiO_2} \quad (2.37)$$

The free energy changes of electron injection ( $\Delta G_{inject}$ )<sup>76</sup>, dye regeneration ( $\Delta G_{reg}$ ) and dye recombination ( $\Delta G_{rec}$ ) can be defined as the following equations<sup>77</sup>.

$$\Delta G_{inject} = E_{CB}^{TiO_2} - E^{dye*} \quad (2.38)$$

$$\Delta G_{reg} = E^{dye} - E_{redox}^{I_3^-/I^-} \quad (2.39)$$

$$\Delta G_{rec} = E^{dye} - E_{CB}^{TiO_2} \quad (2.40)$$

where  $E_{redox}^{I_3^-/I^-}$  is the redox mediator of which the experimental value is -4.80 eV as found in ref<sup>78</sup>. The  $E_{CB}^{TiO_2}$  of -4.00 eV obtained in ref.<sup>76</sup> was used in all related equations.

## CHAPTER III

### COMPUTATIONAL DETAILS

#### 3.1 The optimized structure of $\alpha$ -mangostin

##### 3.1.1 DFT and TD/DFT methods

Structures optimizations of  $\alpha$ -mangostin conformers, their deprotonated and dehydrogenated species were carried out using density functional theory (DFT) method. DFT calculations have been performed with hybrid density functional B3LYP, the Becke's three-parameter exchange functional<sup>79</sup> with the Lee-Yang-Parr correlation functional<sup>80</sup>, using the 6-31+G(d,p)<sup>81</sup> and 6-31G(d) basis sets<sup>82</sup>. All DFT-optimized structures were performed with the GAUSSIAN 09 program<sup>83</sup>. Structure optimizations of all species in acetonitrile and water, solvent-effect computations using the polarizable continuum model (PCM)<sup>84-86</sup> using the CPCM<sup>87-89</sup> method have been used. The molecular cavity model used in the PCM model is the united atoms radii of UFF force field<sup>90</sup>. Based on the B3LYP/6-31+G(d,p), the solvation-effect is therefore so-called CPCM/UFF/B3LYP/6-31+G(d,p) method. The excited state properties for studied compounds were obtained using TD-DFT calculations<sup>91-92</sup> at the CPCM/UFF/B3LYP/6-31+G(d,p) level of theory. Enthalpy ( $H$ ) and Gibbs free energies ( $G$ ) of all compounds were obtained from their vibration frequency computations at 298.15 K and standard pressure. The molecular graphics of all related species were generated with the MOLEKEL 5.4.0.8 program<sup>93</sup>.

##### 3.1.2 Periodic DFT method

All quantum-mechanical calculations were carried out using the CRYSTAL14 software packages<sup>94</sup> implementing a periodic LCAO (linear combination of atomic orbitals) approach with atom-centered Gaussian type basis functions. The B3LYP hybrid functional has been selected with basis sets, The basis sets (6-21G)<sup>95</sup>,



(8-411d1G)<sup>96</sup> and (3-1p1G)<sup>94</sup> were employed for C, O and H atoms, respectively. A Monkhorst-Pack shrinking factor of  $2 \times 2 \times 1$   $k$ -point was used to sample the Brillouin zone. The tolerances for geometry optimization convergence have been set to the default values and the default truncation thresholds of  $10^{-6}$ ,  $10^{-6}$ ,  $10^{-6}$ ,  $10^{-6}$  and  $10^{-12}$  for the coulomb-exchange screening tolerances. Fock/Kohn-Sham matrices mixing was set to 30.

### 3.1.3 DFTB method

Optimized structures of conformers of the  $\alpha$ -mangostin, their deprotonated and dehydrogenated species were carried out using self-consistent charge density functional tight-binding (SCC-DFTB) periodic calculations. All SCC-DFTB calculations were performed with the code of DFTB+ version 1.3<sup>97</sup>. Parameter sets "mio-0-1"<sup>97</sup> for H, C atoms. All SCC-DFTB calculations, the atomic positions were relaxed until the forces in the system became smaller than  $1.9 \times 10^{-5}$  eV/Å which SCC tolerance were smaller than  $1.0 \times 10^{-5}$  e.

### 3.2 Simulation of UV-Vis spectrum

UV-Vis spectra of all related conformers were simulated from calculated oscillator strengths using Gaussian functions using GaussSum 3.0 software<sup>98</sup>. The full width at half-maximum (FWHM) of  $2,700 \text{ cm}^{-1}$  was selected for making gaussian curves from oscillator strengths values to construction of the spectrum. The maximum wavelengths of spectrum were obtained from the simulated UV-Vis spectrum. As spectral absorptivity of the mixture is a total spectral absorptivities of all components, the simulated UV-Vis spectral absorptivity of the mixture as the linear combination of its components is assumed as shown in Eq (3.1).

$$\varepsilon_j^{mixture} = \sum_i^n \varepsilon_{ji} f_{n_i} \quad (3.1)$$

where  $\varepsilon_j^{mixture}$  is the molar extinction coefficient of the mixture at the wavelength  $j$ .  $\varepsilon_{ji}$  and  $f_{n_i}$  are the molar extinction coefficient and mole fraction of the conformer  $i$  at the wavelength  $j$ , respectively.  $N$  is the number of conformers in system. The mole fraction of conformer can be obtained from its equilibrium constant which is computed using Eq (3.2).

$$K = \exp(-\Delta G_{298}^\circ / RT) \quad (3.2)$$

where  $\Delta G_{298}^\circ$  is Gibbs free energy change of interconversion of two species.  $R$  ( $1.985 \times 10^{-3}$  kcal K<sup>-1</sup> mol<sup>-1</sup>) and  $T$  (298.15 K) are gas constant and absolute temperature, respectively.

As number of equilibrium constants ( $K_{i-i+1}$ ) of sequential ( $N-1$ ) steps of  $N$  conformers (Conformers  $1 \rightarrow 2 \rightarrow 3 \rightarrow \dots \rightarrow N$ ), mole fraction of the conformer ( $f_{n_i}$ ) can be obtained by Eq (3.3).

$$f_{n_i} = \frac{n_i}{\sum_{i=1}^N n_i} \quad (3.3)$$

where  $n_i$  is mole of conformer  $i$  of all  $N$  conformers or  $n_i = \prod_{j=0}^{j=i} K_{j-j+1}$  whereas  $K_{0-1}$  is identical to  $n_1$  which is mole of the conformeric reactant at the first step.  $n_1$  can be any value of mole which is generally assigned to unity.

## CHAPTER IV

### RESULTS AND DISCUSSION

#### 4.1 Conformation, deprotonation and dehydrogenation of $\alpha$ -mangostin

##### 4.1.1 Conformers of the $\alpha$ -mangostin

The optimized structures of five conformers in gas phase computed by B3LYP/6-31+G(d,p), periodic B3LYP and DFTB methods are shown in Figure 5. The last two methods resulted structures of these conformers that are very similar to those obtained from the B3LYP/6-31+G(d,p) method. Energies of frontier orbitals and energy gaps of five conformers of the  $\alpha$ -mangostin in various media, based on their B3LYP/6-31+G(d,p)-optimized structures are shown in Table 2. Based on the energy gaps obtained by B3LYP/6-31+G(d,p) method in all three media, reactivities of Conformers 2, 3 and 4 are remarkably higher than Conformers 1 and 5.

Either B3LYP/6-31+G(d,p) or periodic B3LYP method, the stabilise of these five conformers are in order: Conformer 2 > Conformer 3 > Conformer 4 > Conformer 5 > Conformer 1, but stabilise computed by periodic DFTB are in order: Conformer 3 ~ Conformer 2 > Conformer 4 > Conformer 5 > Conformer 1, as shown in Table 3. The Conformers 2 and 3 are reverse order for periodic DFTB calculations but they are not significantly different. However, different structures between Conformers 2 and 3 are hardly observed as shown in Figure 5. Due to relative energies of these five conformers, three conformers (Conformers 2, 3 and 4) of which energy differences are less than 3.5 kcal/mol, dominantly exist in the nature. Conformers 2, 3 and 4 are therefore accounted into as a mixture of the  $\alpha$ -mangostin solution.

Nevertheless, orientations of all functional groups which noted by G1, G2, G3, G4, G5 and G6 as defined Figures 5 and 6, for each conformer of the  $\alpha$ -mangostin either obtained by different theory or in different media, point in the same orientations of which sets are listed in Table 4. It shows that G2 orientation becomes the most

effective group on stability of these conformers namely  $G2 = \beta$  and  $G2 = \alpha$  are less stable (Conformers 1 and 5) and much more stable conformers (Conformers 2, 3 and 4), respectively. As stability of conformer depends on orientation of existing functional groups,  $G2 = \beta$  and  $G2 = \alpha$  may cause by high repulsion between O1 and O2, and attraction between O1 and H1<sub>O2</sub>, respectively. As (G1, G2, G3) set of functional groups of Conformer 2 ( $\alpha, \alpha, \alpha$ ), Conformer 3 ( $\beta, \alpha, \beta$ ), and Conformer 4 ( $\alpha, \alpha, \beta$ ) compared with their relative stability energies either in vacuo, acetonitrile or water are in the same order: Conformer 2 > Conformer 3 > Conformer 4, G1 orientations slightly affect to stabilities of Conformer 3 and Conformer 4.

#### 4.1.2 Deprotonations and dehydrogenation of $\alpha$ -mangostin

Total and relative energies of deprotonated and dehydrogenated species of the Conformer 2 of  $\alpha$ -mangostin based on three hydroxyl hydrogen atoms (H1, H2 and H3 as labeled in Figure 5) were obtained by three different methods. Total energies of the  $\alpha$ -mangostin (denoted by LOH), their deprotonated (LO<sup>-</sup>) and dehydrogenated (LO<sup>•</sup>) and their relative energies are tabulated in Table 3. The stabilities of deprotonated and dehydrogenated species of the Conformer 2 were found in same orders: Conformer 2(H3)<sup>-</sup> > Conformer 2(H2)<sup>-</sup> > Conformer 2(H1)<sup>-</sup> and Conformer 2(H3)<sup>•</sup> > Conformer 2(H2)<sup>•</sup> > Conformer 2(H1)<sup>•</sup>, respectively. Total and relative energies deprotonated and dehydrogenated species of the Conformer 2 of  $\alpha$ -mangostin in vacuo, acetonitrile and water, computed based on B3LYP/6-31+G(d,p) method are shown in Table 5. It shows the same orders: Conformer 2(H3)<sup>-</sup> > Conformer 2(H2)<sup>-</sup> > Conformer 2(H1)<sup>-</sup> for deprotonated species and Conformer 2(H3)<sup>•</sup> > Conformer 2(H2)<sup>•</sup> > Conformer 2(H1)<sup>•</sup> for dehydrogenated species. It can be concluded that the H3 of deprotonated and dehydrogenated species are the most stable species. According to reaction of the  $\alpha$ -mangostin with other substrate or material surface are considered, its Conformer 2(H3)<sup>-</sup> and Conformer 2(H3)<sup>•</sup> species are expected to be involved.

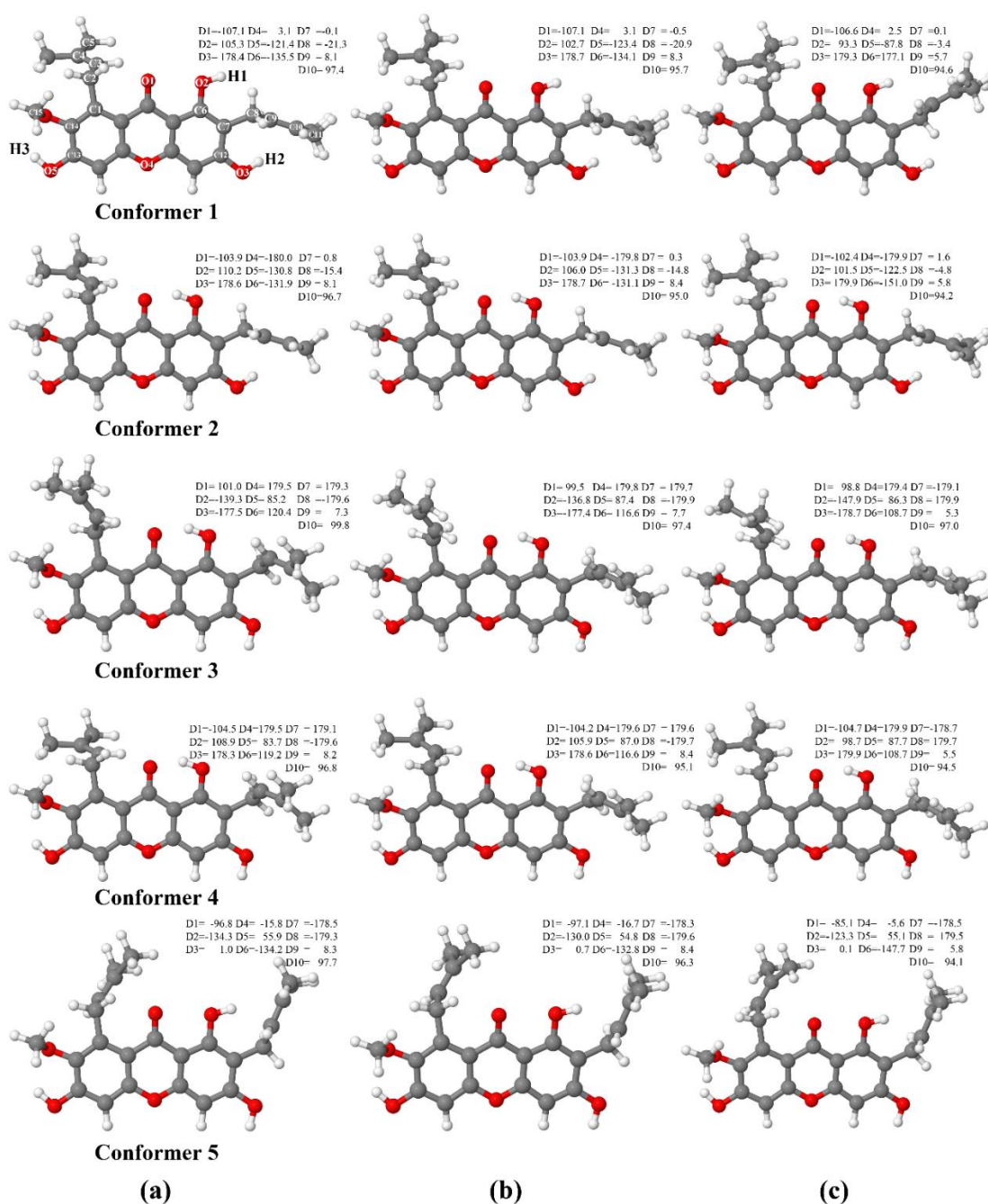


**Figure 5.** Optimized structures of five conformers of the  $\alpha$ -mangostin in gas phase obtained by (a) B3LYP/6-31+G(d,p), (b) periodic DFT and (c) periodic DFTB computations. Notes: D1=C14-C1-C2-C3, D2=C1-C2-C3-C4, D3=C2-C3-C4-C5, D4=C7-C6-O2-H1, D5=C6-C7-C8-C9, D6=C7-C8-C9-C10, D7=C8-C9-C10-C11, D8=C7-C12-O3-H2, D9=C14-C13-O5-H3, D10=C13-C14-O6-C15.

**Table 2.** Energies of frontier orbitals and energy gaps of five conformers of the  $\alpha$ -mangostin, their deprotonated and dehydrogenated species in various media, based on their B3LYP/6-31G+(d,p)-optimized structures.

Species	Vacuo			Acetonitrile			Water		
	$E_{\text{HOMO}}^{\text{a}}$	$E_{\text{LUMO}}^{\text{a}}$	$E_{\text{gap}}^{\text{a}}$	$E_{\text{HOMO}}^{\text{a}}$	$E_{\text{LUMO}}^{\text{a}}$	$E_{\text{gap}}^{\text{a}}$	$E_{\text{HOMO}}^{\text{a}}$	$E_{\text{LUMO}}^{\text{a}}$	$E_{\text{gap}}^{\text{a}}$
<i>LOH form:</i>									
Conformer 1	-5.96	-1.48	4.49	-6.16	-1.80	4.36	-6.16	-1.81	4.36
Conformer 2	-5.96	-1.86	4.11	-6.14	-2.04	4.10	-6.15	-2.04	4.10
Conformer 3	-5.97	-1.91	4.06	-6.13	-2.03	4.10	-6.13	-2.03	4.10
Conformer 4	-5.98	-1.93	4.05	-6.13	-2.04	4.09	-6.13	-2.04	4.09
Conformer 5	-5.96	-1.48	4.48	-6.15	-1.79	4.36	-6.15	-1.80	4.36
<i>LO<sup>-</sup> form:</i>									
Conformer 2-(H1) <sup>-</sup>	-1.50	1.72	3.22	-4.84	-1.20	3.64	-4.90	-1.25	3.65
Conformer 2-(H2) <sup>-</sup>	-1.91	1.31	3.22	-5.13	-1.44	3.69	-5.19	-1.49	3.70
Conformer 2-(H3) <sup>-</sup>	-1.99	1.49	3.48	-5.16	-1.40	3.76	-5.22	-1.45	3.77
<i>LO<sup>•</sup> form:</i>									
Conformer 2-(H1) <sup>•</sup>	-6.12	-1.71	4.41	-6.37	-1.84	4.52	-6.37	-1.85	4.52
Conformer 2-(H2) <sup>•</sup>	-6.00	-2.27	3.72	-6.43	-2.17	4.26	-6.44	-2.17	4.26
Conformer 2-(H3) <sup>•</sup>	-6.34	-2.19	4.15	-6.10	-2.11	3.99	-6.10	-2.11	3.99

<sup>a</sup> In eV.

**Table 3.** Total energies of  $\alpha$ -mangostin (LOH) conformers, their deprotonated (LO<sup>-</sup>), dehydrogenated (LO<sup>•</sup>) species and relative energies in gas phase, computed at various methods.

Species	B3LYP/6-31+G (d,p)		Periodic B3LYP <sup>a</sup>		Periodic DFTB	
	$E_{\text{total}}$ <sup>b,c</sup>	$\Delta E_{\text{rel}}$ <sup>c,d</sup>	$E_{\text{total}}$ <sup>b</sup>	$\Delta E_{\text{rel}}$ <sup>d</sup>	$E_{\text{total}}$ <sup>b</sup>	$\Delta E_{\text{rel}}$ <sup>d</sup>
<i>LOH form:</i>						
Conformer 1	-1381.156459	17.47	-1381.03830679	17.68	-70.759042776	10.58
Conformer 2	-1381.184299	0.00	-1381.06648462	0.00	-70.775106084	0.50
Conformer 3	-1381.181098	2.01	-1381.06264295	2.41	-70.775905739	0.00
Conformer 4	-1381.180276	2.52	-1381.06103725	3.42	-70.774191851	1.08
Conformer 5	-1381.159030	15.86	-1381.04077787	16.13	-70.761559161	9.00
<i>LO<sup>-</sup> form:</i>						
Conformer 2-(H1) <sup>-</sup>	-1380.634872	21.07	-1380.48814862	20.02	-70.330672853	14.57
Conformer 2-(H2) <sup>-</sup>	-1380.662334	3.83	-1380.51480367	3.30	-70.340798466	8.22
Conformer 2-(H3) <sup>-</sup>	-1380.668443	0.00	-1380.52005491	0.00	-70.353898110	0.00
<i>LO<sup>•</sup> form:</i>						
Conformer 2-(H1) <sup>•</sup>	-1380.971827	14.74	-1380.38447247	15.85	-70.330401132	5.28
Conformer 2-(H2) <sup>•</sup>	-1380.986525	5.52	-1380.39842330	7.09	-70.329468832	5.86
Conformer 2-(H3) <sup>•</sup>	-1380.995324	0.00	-1380.40972956	0.00	-70.338810485	0.00

<sup>a</sup> Based on the CRYSTAL14 software, with m-6-311G(d)\_Heyd\_2005 basis set for carbon, oxygen atoms and pob\_TZVP\_2012 basis set for hydrogen atom.

<sup>b</sup> In au.

<sup>c</sup> Based on ZPVE correction.

<sup>d</sup> In kcal/mol, compared with the most stable conformer.

**Table 4.** Identification based on functional group orientations of conformers.

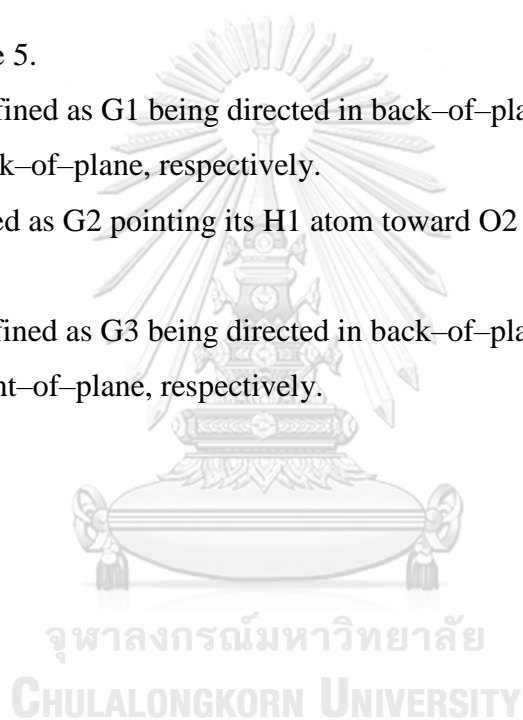
Conformer	Orientation of functional group		
	<b>G1</b> <sup>a,b</sup>	<b>G2</b> (-OH1) <sup>a,c</sup>	<b>G3</b> <sup>a,d</sup>
<b>1</b>	$\alpha$	$\beta$	$\alpha$
<b>2</b>	$\alpha$	$\alpha$	$\alpha$
<b>3</b>	$\beta$	$\alpha$	$\beta$
<b>4</b>	$\alpha$	$\alpha$	$\beta$
<b>5</b>	$\alpha'$	$\beta$	$\beta'$

<sup>a</sup> Defined in Figure 5.

<sup>b</sup>  $\alpha$ ,  $\beta$  and  $\alpha'$  are defined as G1 being directed in back-of-plane, front-of-plane and second type of back-of-plane, respectively.

<sup>c</sup>  $\alpha$  and  $\beta$  are defined as G2 pointing its H1 atom toward O2 atom and G1, respectively.

<sup>d</sup>  $\alpha$ ,  $\beta$  and  $\beta'$  are defined as G3 being directed in back-of-plane, front-of-plane and second type of front-of-plane, respectively.





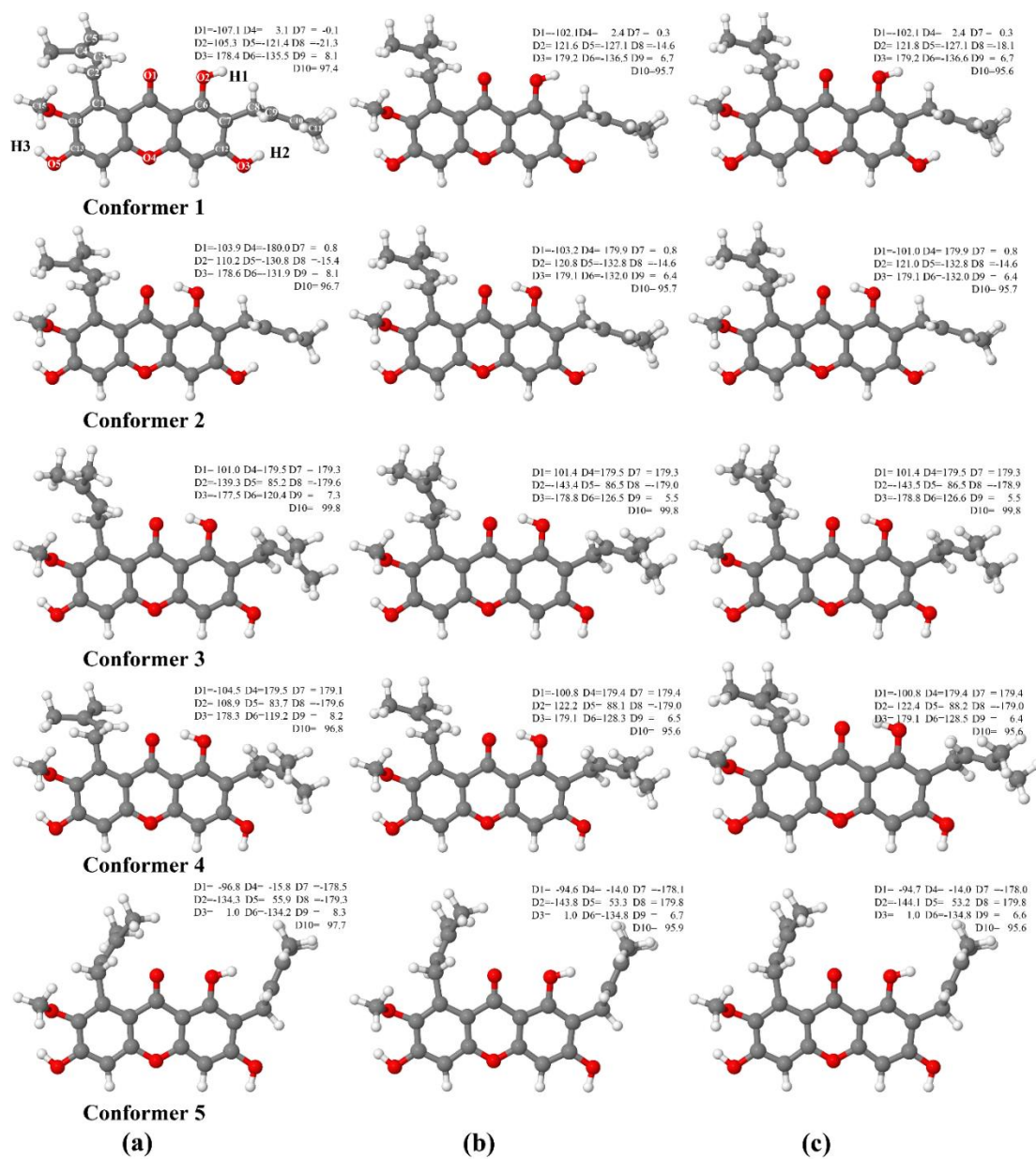


**Figure 6.** B3LYP/6-31+G(d,p)-optimized structures of five conformers of the  $\alpha$ -mangostin in (a) gas phase, (b) acetonitrile and (c) water. Notes: D1=C14-C1-C2-C3, D2=C1-C2-C3-C4, D3=C2-C3-C4-C5, D4=C7-C6-O2-H1, D5=C6-C7-C8-C9, D6=C7-C8-C9-C10, D7=C8-C9-C10-C11, D8=C7-C12-O3-H2, D9=C14-C13-O5-H3, D10=C13-C14-O6-C15.

**Table 5.** Total energies of  $\alpha$ -mangostin (LOH) conformers, their deprotonated ( $\text{LO}^-$ ), dehydrogenated ( $\text{LO}^*$ ) species and relative energies in various media, computed based on B3LYP/6-31+G(d,p) method.

Species	Vacuo <sup>a</sup>		Acetonitrile <sup>b</sup>		Water <sup>b</sup>	
	$E_{\text{total}}^{\text{c}}$	$\Delta E_{\text{rel}}^{\text{d}}$	$E_{\text{total}}^{\text{c}}$	$\Delta E_{\text{rel}}^{\text{d}}$	$E_{\text{total}}^{\text{c}}$	$\Delta E_{\text{rel}}^{\text{d}}$
<i>LOH form:</i>						
Conformer 1	-1381.156459	17.47	-1381.177983	12.82	-1381.178386	12.74
Conformer 2	-1381.184299	0.00	-1381.198411	0.00	-1381.198683	0.00
Conformer 3	-1381.181098	2.01	-1381.196775	1.03	-1381.197074	1.01
Conformer 4	-1381.180276	2.52	-1381.196495	1.20	-1381.196805	1.18
Conformer 5	-1381.159030	15.86	-1381.179452	11.90	-1381.179847	11.82
<i>LO<sup>-</sup> form:</i>						
Conformer 2-(H1) <sup>-</sup>	-1380.634872	21.07	-1380.721983	13.71	-1380.723615	13.55
Conformer 2-(H2) <sup>-</sup>	-1380.662334	3.83	-1380.740658	2.00	-1380.742102	1.95
Conformer 2-(H3) <sup>-</sup>	-1380.668443	0.00	-1380.743839	0.00	-1380.745204	0.00
<i>LO<sup>*</sup> form:</i>						
Conformer 2-(H1) <sup>*</sup>	-1380.971827	14.74	-1380.553449	8.66	-1380.553893	8.53
Conformer 2-(H2) <sup>*</sup>	-1380.986525	5.52	-1380.560962	3.94	-1380.561246	3.92
Conformer 2-(H3) <sup>*</sup>	-1380.995324	0.00	-1380.567243	0.00	-1380.567492	0.00

<sup>a</sup> Based on B3LYP/6-31+G(d,p) calculation with ZPVE correction.

<sup>b</sup> Based on CPCM/UFF/B3LYP/6-31+G(d,p) calculation with ZPVE correction.

<sup>c</sup> In au.

<sup>d</sup> In kcal/mol, compared with the most stable conformer.

#### 4.2 The most three stable conformers of the $\alpha$ -mangostin in various media

As Conformers 2, 3 and 4 are previously mentioned as the most three stable conformers, they are therefore considered to exist in the  $\alpha$ -mangostin solution as their mixture. Electrostatic potential maps of three most stable conformers of the  $\alpha$ -mangostin in gas phase, acetonitrile and water, computed at the B3LYP/6-31+G(d,p) are shown in Figure 7.

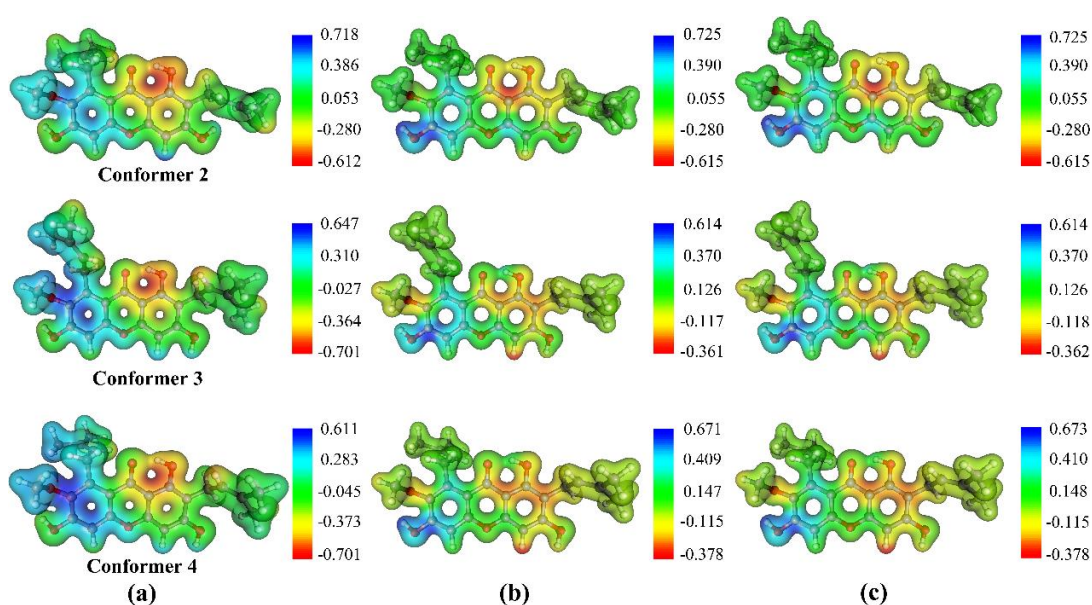


**Figure 7.** Electrostatic potential maps with iso-surface value of  $0.03 \text{ e } \text{\AA}^{-3}$ , showing charge density distribution in three most stable conformers of the  $\alpha$ -mangostin in (a) gas phase, (b) acetonitrile and (c) water, based on their B3LYP/6-31+G(d,p)-optimized structures.

#### 4.2.1 Equilibrium constants of interconversion between conformers

Based on assumption of Conformers 2, 3 and 4 are three species that exist in the nature, these three major conformers are therefore theoretically investigated in terms of their equilibrium constants to acquire their mole fraction ( $f_n$ ) which were obtained by Eq (3.3). The equilibrium constants between Conformers 2, 3 and 4 ( $K_{2-4}$ ,  $K_{4-3}$  and  $K_{2-3}$ ) at 298 K, 1 atm (in vacuo, acetonitrile and water), computed from Gibbs free energy change ( $\Delta G_{298}^\circ$ ) of their interconversions are shown in Table 6. All  $\Delta G_{298}^\circ$  of interconversions of Conformer 2  $\rightarrow$  4, Conformer 4  $\rightarrow$  3 and Conformer 2  $\rightarrow$  3 were computed from Gibbs free energies of Conformers 2, 3 and 4 as listed in Table 7. Their related parameters including molecular descriptions are graphically shown in Figure 8. The reaction energy and enthalpy changes of interconversion between three major conformers in various media are shown in Table 8.

**Table 6.** The Gibbs free energy changes of interconversion between three major conformers and their equilibrium constants at 298 K, 1 atm, in various media.

Interconversion	$\Delta G_{298}^{\circ}$ <sup>a</sup>	$K$ <sup>b</sup>
<i>Gas Phase:</i>		
Conformer 2 $\rightarrow$ 4	2.605	$1.23 \times 10^{-2}$
Conformer 4 $\rightarrow$ 3	-0.633	$2.91 \times 10^0$
Conformer 2 $\rightarrow$ 3	1.972	$3.58 \times 10^{-2}$
<i>Acetonitrile:</i>		
Conformer 2 $\rightarrow$ 4	1.083	$1.61 \times 10^{-1}$
Conformer 4 $\rightarrow$ 3	-0.019	$1.03 \times 10^0$
Conformer 2 $\rightarrow$ 3	1.064	$1.66 \times 10^{-1}$
<i>Water:</i>		
Conformer 2 $\rightarrow$ 4	1.120	$1.51 \times 10^{-1}$
Conformer 4 $\rightarrow$ 3	-0.020	$1.03 \times 10^0$
Conformer 2 $\rightarrow$ 3	1.100	$1.56 \times 10^{-1}$

<sup>a</sup> In kcal/mol.

<sup>b</sup> Computed by  $K = \exp(-\Delta G_{298}^{\circ} / RT)$ ,  $T=298.15$  K,  $R = 1.985 \times 10^{-3}$  kcal K<sup>-1</sup> mol<sup>-1</sup>.

**Table 7.** Energetic and thermodynamics of three most stable conformers in various media and of their molecule distribution.

System	$E_{ZPE}^a$	$H^b$	$G^b$	$f_n^c$	$\%on^d$
<i>Gas Phase:</i>					
Conformer 2	-1381.184299	-1381.153721	-1381.246282	$9.54 \times 10^{-1}$	95.4
Conformer 3	-1381.181098	-1381.150390	-1381.243140	$3.41 \times 10^{-2}$	3.4
Conformer 4	-1381.180276	-1381.149607	-1381.242131	$1.17 \times 10^{-2}$	1.2
<i>Acetonitrile:</i>					
Conformer 2	-1381.198411	-1381.167720	-1381.260537	$7.54 \times 10^{-1}$	75.4
Conformer 3	-1381.196775	-1381.165998	-1381.258842	$1.25 \times 10^{-1}$	12.5
Conformer 4	-1381.196495	-1381.165751	-1381.258811	$1.21 \times 10^{-1}$	12.1
<i>Water:</i>					
Conformer 2	-1381.198683	-1381.167984	-1381.260892	$7.65 \times 10^{-1}$	76.5
Conformer 3	-1381.197074	-1381.166295	-1381.259139	$1.19 \times 10^{-1}$	11.9
Conformer 4	-1381.196805	-1381.166062	-1381.259107	$1.15 \times 10^{-1}$	11.5

<sup>a</sup> Based on the B3LYP/6-31+G(d,p) calculations with ZPVE correction, in kcal/mol.

<sup>b</sup> Derived from the B3LYP/6-31+G(d,p) calculations with ZPVE correction at 298.15K, in kcal/mol.

<sup>c</sup> Mole fractions of three major conformers (unitless), derived from equilibrium constants ( $K$ ) of their interconversion.

<sup>d</sup> In mole percent of three conformers.

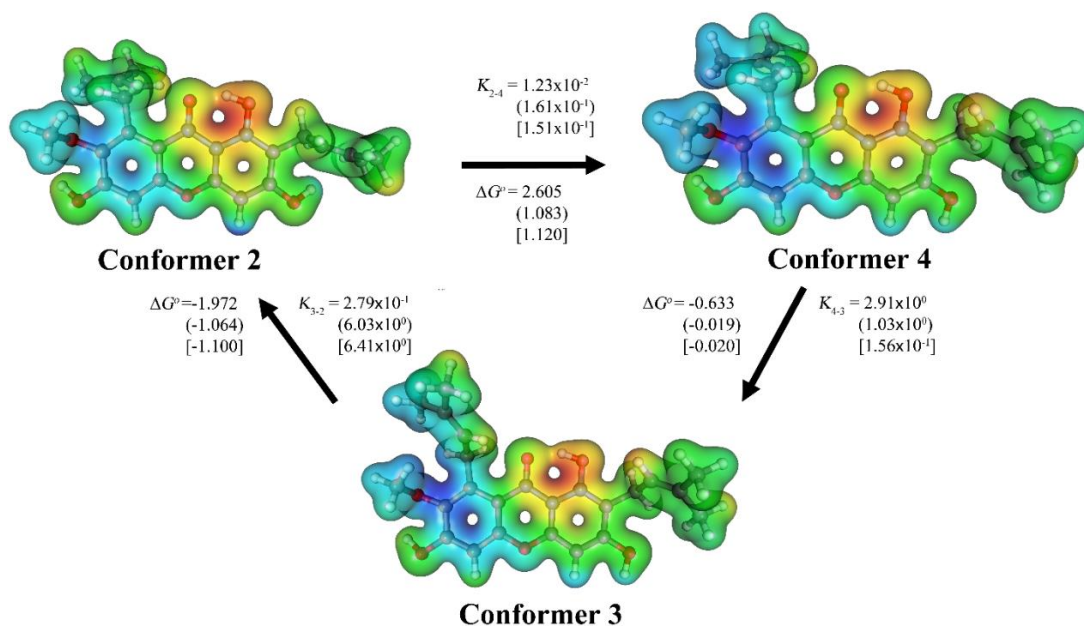
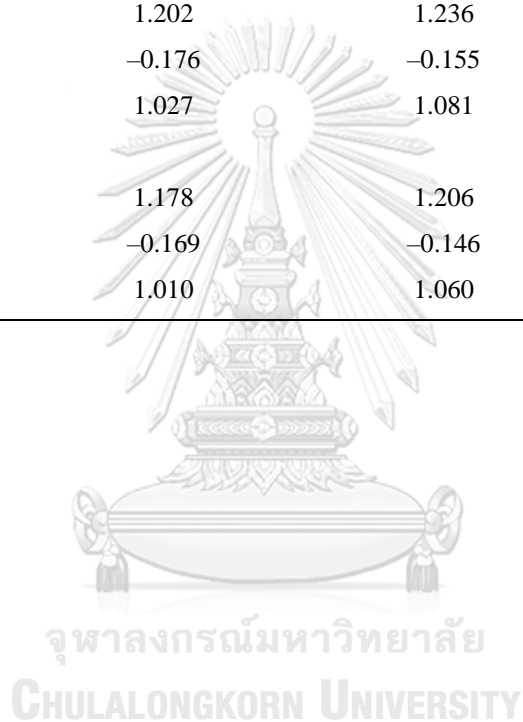


**Figure 8.** Interconversions of three major conformers of the  $\alpha$ -mangostin. Values in parentheses and square brackets are systems in acetonitrile and water, respectively otherwise in gas phase. Gibbs free energy changes are in kcal/mol and equilibrium constants are unitless.

**Table 8.** The reaction energy, enthalpy and Gibbs free energy changes of interconversion between three major conformers at 298 K, 1 atm, in various media.

Interconversion	$\Delta E^a$	$\Delta H_{298}^\circ{}^a$	$\Delta G_{298}^\circ{}^a$
<i>Gas Phase:</i>			
Conformer 2 $\rightarrow$ 4	2.524	2.582	2.605
Conformer 4 $\rightarrow$ 3	-0.516	-0.491	-0.633
Conformer 2 $\rightarrow$ 3	2.009	2.090	1.972
<i>Acetonitrile:</i>			
Conformer 2 $\rightarrow$ 4	1.202	1.236	1.083
Conformer 4 $\rightarrow$ 3	-0.176	-0.155	-0.019
Conformer 2 $\rightarrow$ 3	1.027	1.081	1.064
<i>Water:</i>			
Conformer 2 $\rightarrow$ 4	1.178	1.206	1.120
Conformer 4 $\rightarrow$ 3	-0.169	-0.146	-0.020
Conformer 2 $\rightarrow$ 3	1.010	1.060	1.100

<sup>a</sup> In kcal/mol.





#### 4.2.2 Simulated UV–Vis spectra of the mixture of dye conformers

Based on assumption that Conformers 2, 3 and 4 are only existing in the nature, these three major conformers are therefore theoretically investigated in terms of their equilibria and UV–Vis spectra which are composed of three major components. Besides investigating of these three major conformers in gas phase, systems in acetonitrile and in water were selected as representatives of aprotic and protic solvents, respectively. Major transitions of three most stable conformers of  $\alpha$ -mangostin in gas phase, acetonitrile and water are shown in Table 9. The three apparent maximum absorption wavelengths, ( $\lambda_{\max}^1$ ,  $\lambda_{\max}^2$  and  $\lambda_{\max}^3$ ) of mixtures in gas phase, acetonitrile and water are (259.88, 306.75 and 348.43 nm), (259.07, 311.33 and 350.63 nm) and (259.07, 311.33 and 350.63 nm), respectively. The pattern of simulated UV–Vis spectra of these three mixtures in gas phase, acetonitrile and water are very similar to experiments in various solvents<sup>12</sup>. Based on the  $\lambda_{\max}^1$ , the major transitions for all three conformers in all media were found to be the electronic transitions of HOMO to LUMO+1 (denoted by H→L+1) as shown in Table 10. The oscillator strengths of the UV–Vis spectra of three most stable conformers in various media are in order: Conformer 2 > Conformer 4 > Conformer 3. This means that the molar absorptivity of the Conformer 2 is the highest as compared within all three media.

**Table 9.** Major transitions of three maximum wavelengths of the three most stable conformers of  $\alpha$ -mangostin in various media.

Species	First peak		Second peak		Third peak	
	$\lambda_{\max}^1$ <sup>a</sup>	MT <sup>b,c</sup>	$\lambda_{\max}^2$ <sup>a</sup>	MT <sup>b,c</sup>	$\lambda_{\max}^3$ <sup>a</sup>	MT <sup>b,c</sup>
<i>Vacuo</i> <sup>d</sup>						
Conformer 2	259.88	H→L+1 (76%)	306.75	H-2→L (66%)	348.43	H→L (97%)
Conformer 3	261.10	H→L+1 (72%)	301.75	H-3→L (49%)	351.37	H→L (95%)
Conformer 4	261.51	H→L+1 (80%)	303.40	H-3→L (51%)	350.63	H→L (95%)
Mixture	259.88	–	306.75	–	348.43	–
<i>Acetonitrile</i> <sup>e</sup>						
Conformer 2	259.07	H→L+1 (80%)	311.92	H-2→L (81%)	350.63	H→L (97%)
Conformer 3	259.07	H→L+1 (80%)	308.45	H-3→L (91%)	352.11	H→L (96%)
Conformer 4	259.47	H→L+1 (82%)	310.75	H-3→L (75%)	352.11	H→L (96%)
Mixture	259.07	–	311.33	–	350.63	–
<i>Water</i> <sup>e</sup>						
Conformer 2	258.67	H→L+1 (80%)	311.92	H-2→L (81%)	352.11	H→L (97%)
Conformer 3	259.07	H→L+1 (80%)	308.45	H-3→L (91%)	352.11	H→L (96%)
Conformer 4	259.47	H→L+1 (82%)	310.75	H-3→L (75%)	351.37	H→L (96%)
Mixture	259.07	–	311.33	–	350.63	–

<sup>a</sup> Derived from simulated absorption spectra, in nm.

<sup>b</sup> Based on the major transition (MT) of electron for each peak.

<sup>c</sup> H and L stand for HOMO and LUMO, respectively.

<sup>d</sup> Based on the TD/B3LYP/6-31+G(d,p) calculation.

<sup>e</sup> Based on the TD/CPCM/UHF/B3LYP/6-31+G(d,p) calculations.

**Table 10.** The wavelength of maximum absorptivity ( $\lambda_{\max}^1$ ) and oscillator strengths ( $f$ ) of the UV–Vis spectra of three most stable conformers in various media.

Species	$\lambda_{\max}^1$ <sup>c</sup>	MT <sup>c,d</sup>	$f^c$
<i>Vacuo</i> <sup>a</sup>			
Conformer 2	259.38	H→L+1 (76%)	0.6119
Conformer 3	260.59	H→L+1 (72%)	0.4890
Conformer 4	261.57	H→L+1 (80%)	0.5525
<i>Acetonitrile</i> <sup>b</sup>			
Conformer 2	258.52	H→L+1 (80%)	0.8143
Conformer 3	258.60	H→L+1 (80%)	0.7660
Conformer 4	259.02	H→L+1 (82%)	0.7924
<i>Water</i> <sup>b</sup>			
Conformer 2	258.39	H→L+1 (80%)	0.8139
Conformer 3	258.47	H→L+1 (80%)	0.7664
Conformer 4	258.88	H→L+1 (82%)	0.7925

<sup>a</sup> Based on the TD/B3LYP/6–31+G(d,p) calculations.

<sup>b</sup> Based on the TD/CPCM/UFF/B3LYP/6–31+G(d,p) calculations.

<sup>c</sup> Based on the maximum oscillator strengths obtained at the TD/B3LYP/6–31+G(d,p) level.

<sup>d</sup> Based on the major transition (MT) of electron.

Spectra of the  $\alpha$ -mangostin in ethanol and methanol (protic solvent) showed their spectral characteristics which comprise of the second peak (as  $\lambda_{\max}^2$ ) and one saddle point (as  $\lambda_{\max}^3$ ) which are located at (316 and 355 nm) and (315 and 355 nm), respectively. Spectra of the  $\alpha$ -mangostin in dichloromethane and ethyl acetate (aprotic solvent) showed remarkable two corresponding spectral peaks which are located at (308 and 355 nm) and (313 and 350 nm), respectively<sup>12</sup>. The simulated UV-Vis spectra of the Conformers 2, 3 and 4 in acetonitrile (aprotic) and water (protic solvent) are confirmed to be good agreement with the experiments.

The UV-Vis spectra of the Conformers 2, 3 and 4 in vacuo, acetonitrile and water were simulated using their corresponding oscillator strengths obtained from TD/B3LYP/6-31+G(d,p) and TD/CPCM/UFF/B3LYP/6-31+G(d,p) calculations for vacuo and solvent effect systems, respectively. The orbitals related with electron transitions according to UV-Vis spectra of the Conformers 2, 3 and 4 in vacuo, acetonitrile and water are shown in Figure 9. Each simulated UV-Vis spectra of the pure Conformers 2, 3 and 4 in vacuo, acetonitrile and water are shown in Figure 10. As UV-Vis absorptivities of Conformers 2, 3 and 4 are identically defined, their absorptivities therefore depend their mole fractions. The simulated UV-Vis spectra of a mixture of Conformers 2, 3 and 4 were constructed based on the Eq (3.1). Simulated UV-Vis spectra of the mixtures of three major conformers of the  $\alpha$ -mangostin and their components (Conformers 2, 3 and 4) in vacuo, acetonitrile and water are shown in Figure 11. In gas phase, absorptivity of Conformer 2 much larger than both of Conformers 3 and 4 but in solvents such acetonitrile and water, absorptivity of Conformers 3 and 4 are increased, see Figure 11(b) and (c). Absorptivities of Conformers 2, 3 and 4, in percents of (95.4%, 3.4%, 1.2%) in vacuo, (75.4%, 12.5%, 12.1%) in acetonitrile and (76.5%, 11.9%, 11.5%) in water, are indicated as shown in Table 7. This shows that species distributions of the  $\alpha$ -mangostin in solvents are favoured rather than in gas phase due to the effect of polar environment.

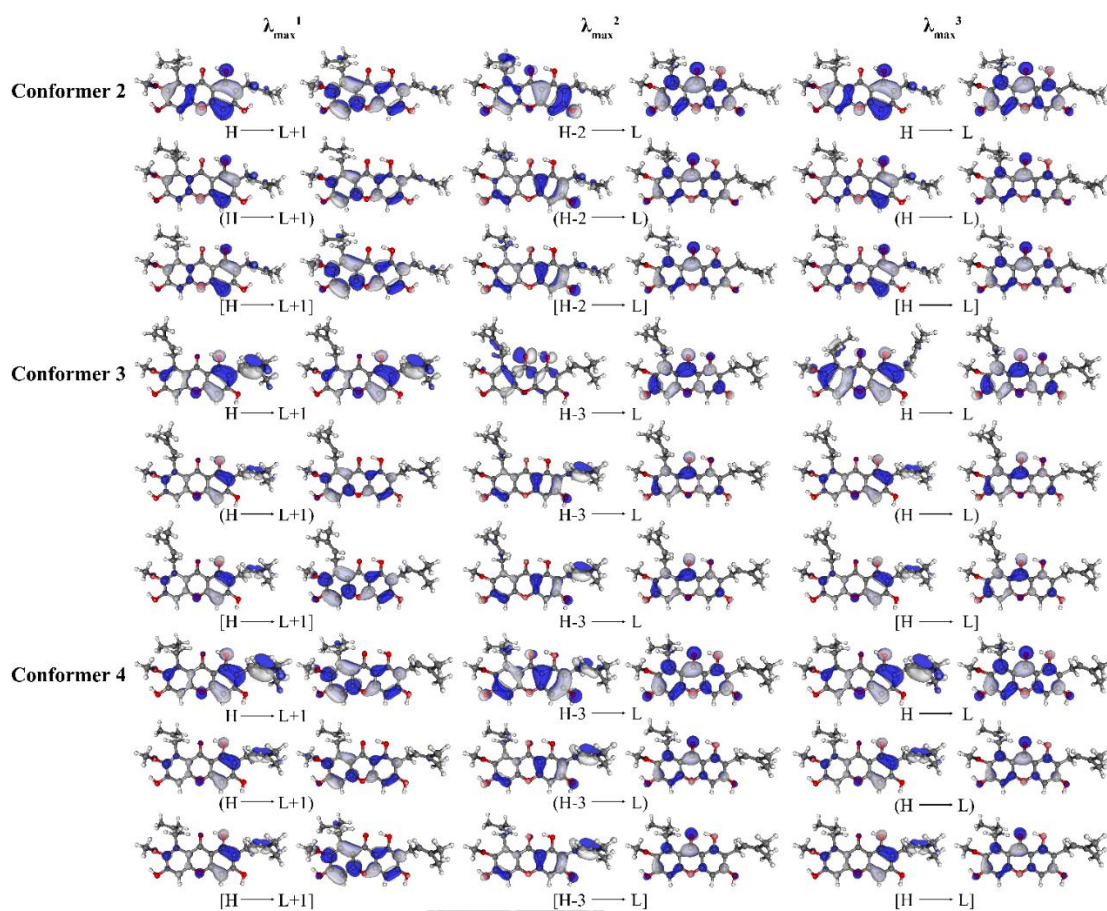


**Figure 9.** The orbitals related with major electron transitions according to UV-Vis spectra of the Conformers 2, 3 and 4 in gas phase (the first row), acetonitrile (the second row) and water (the third row).

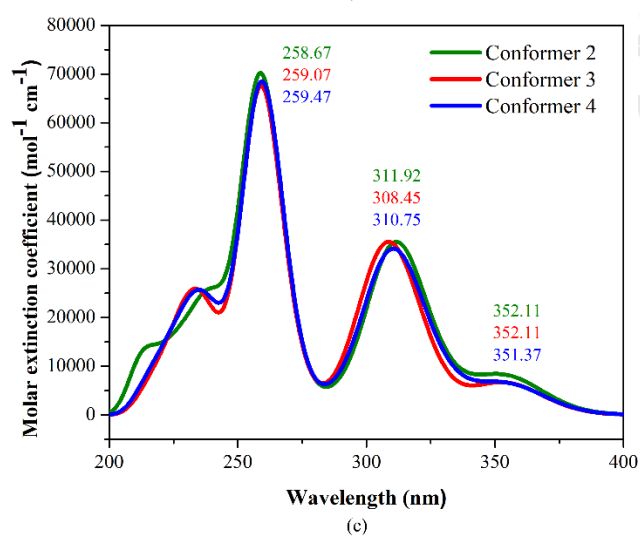
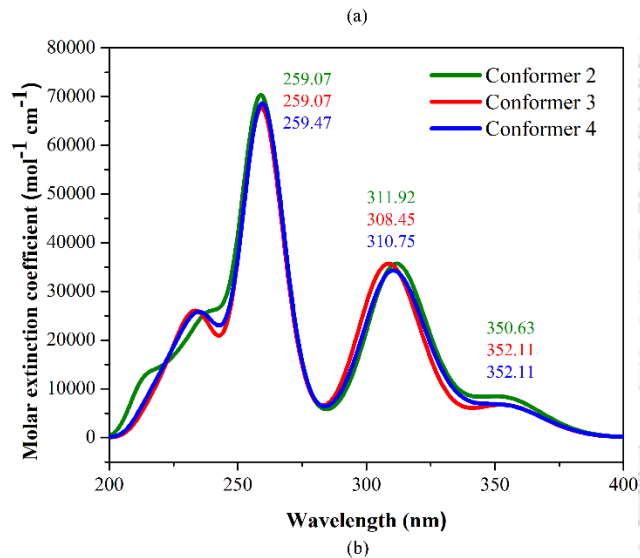
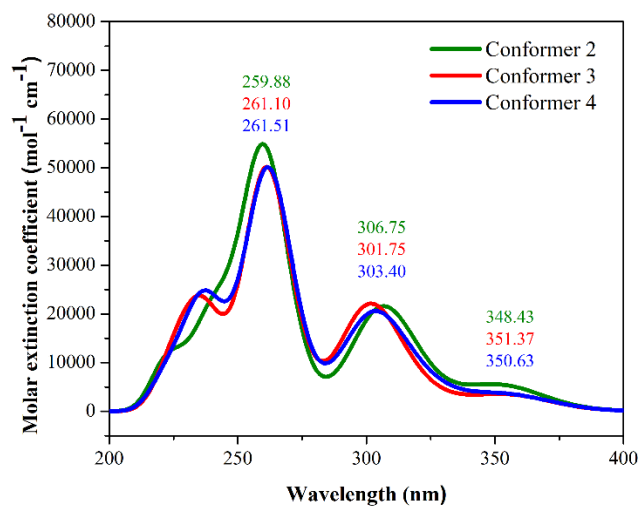
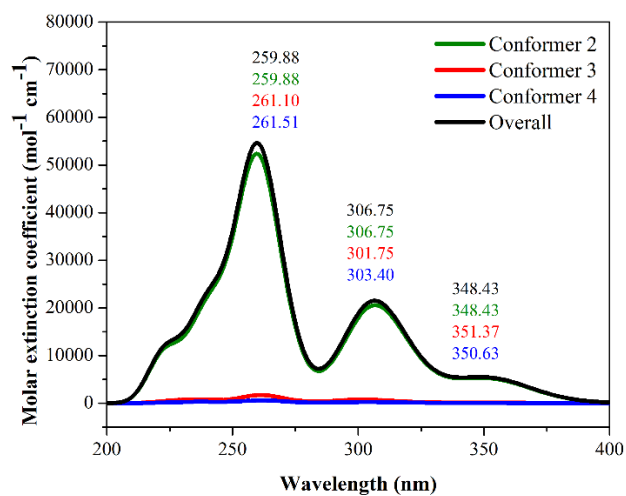
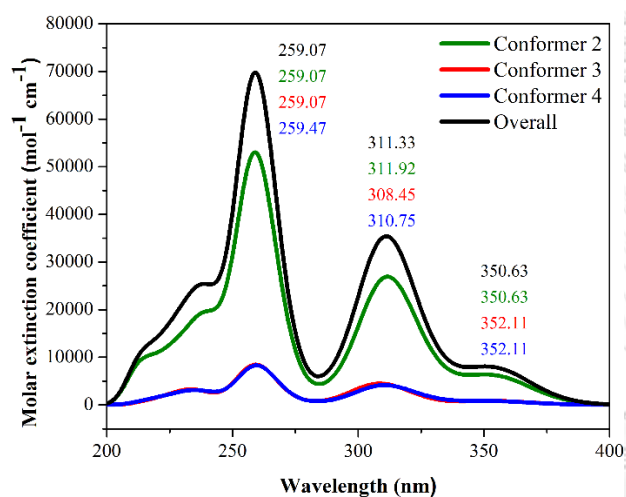


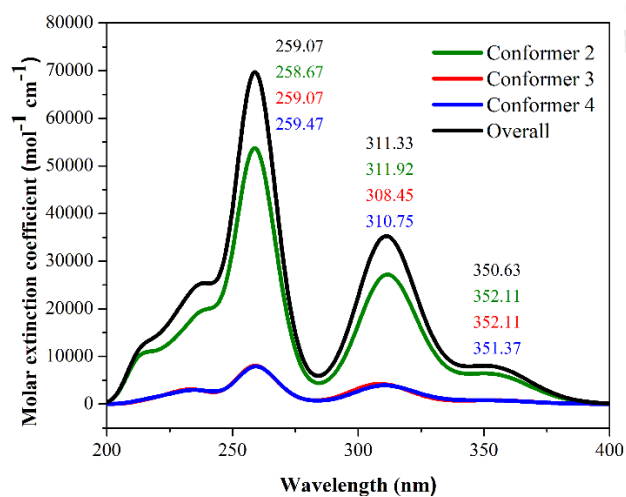
**Figure 10.** The simulated UV/Vis absorption spectra of  $\alpha$ -mangostin conformers (Conformer 2, 3 and 4) in (a) gas phase, (b) acetonitrile and (c) water, based on their corresponding TD/B3LYP/6-31+G(d,p) calculations.



(a)



(b)



(c)

**Figure 11.** Simulated UV–Vis spectra of mixtures of three major conformers of the  $\alpha$ -mangostin and their components (Conformers 2, 3 and 4) in (a) gas phase, (b) acetonitrile and (c) water.

### 4.2.3 Simulated UV–Vis spectra of the Conformer 2 bonded on TiO<sub>2</sub>

As the Conformer 2 is the most stable conformer and the highest populations as mentioned in section “Simulation of UV–Vis spectrum”, Conformer 2 bonded on the TiO<sub>2</sub> (001) surface (denoted by Conformer 2/TiO<sub>2</sub>) as the dominant complex is therefore a representative to be simulated its UV–Vis spectra. The optimized structures of the Conformer 2/TiO<sub>2</sub> in vacuo and in solvents (acetonitrile and water) using B3LYP and CPCM/UFF/B3LYP methods with mixed basis sets (LanL2Dz and 6–31+G(d,p) are for Ti and other atoms, respectively), respectively are shown in Figure 12.

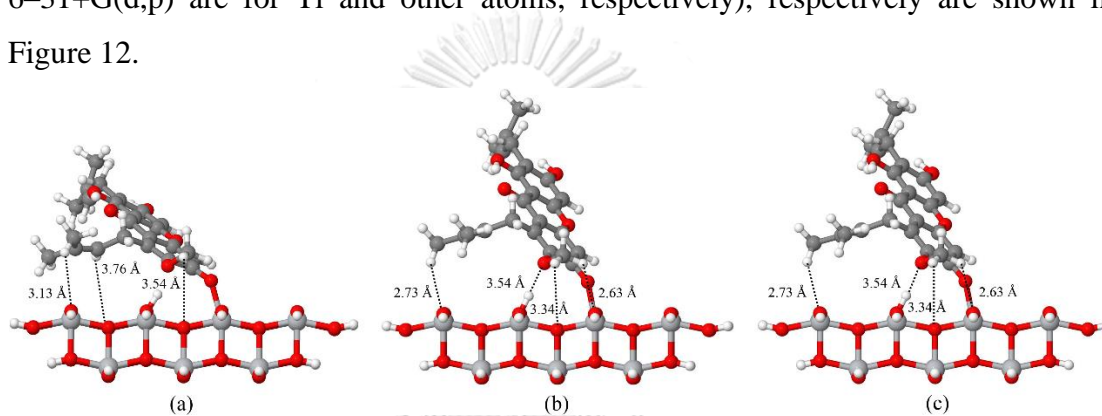


**Figure 12.** Most stable structures of Conformers 2/TiO<sub>2</sub> (001) surface in (a) vacuo, (b) acetonitrile and (c) water. The Conformers 2/TiO<sub>2</sub> in vacuo were optimized using the B3LYP method and in solvents using the CPCM/UFF/B3LYP method, with mixed basis sets (LanL2Dz and 6–31–G+(d,p) are for Ti and other atoms, respectively).

The orbitals related with major electron transitions of the Conformer 2/TiO<sub>2</sub> in vacuo, acetonitrile and water are shown in Figure 13. which shows that major transitions of (HOMO to LUMO+2) and (HOMO to LUMO+13) are in vacuo and solvents (acetonitrile and water), respectively. The simulated UV–Vis spectra of the Conformer 2/TiO<sub>2</sub> in vacuo and solvents are shown in Figure 14. Two spectral peaks of the Conformer 2/TiO<sub>2</sub> in solvents (acetonitrile and water), the maximum wavelength of strong peak (the first) and weak peak (the second saddle point) were found at 549.35 and  $\approx$  710 nm in acetonitrile and at 547.65 and  $\approx$  710 nm in water, respectively. For the Conformer 2/TiO<sub>2</sub> in vacuo was found two strong absorption peaks of which the first and second maximum wavelengths are at  $\approx$  635 and



773.20 nm, respectively. The maximum wavelengths of higher energy peaks of the Conformer 2/TiO<sub>2</sub> in acetonitrile and water were found to be blue-shifted as compared with in the vacuo by 85 and 87 nm, respectively.

The maximum wavelengths of the Conformers 2 dye and the Conformers 2/TiO<sub>2</sub> complexes either in vacuo or solvents are within different ranges of absorption energies. It seems to be that absorption of the high-energy light of the Conformers 2/TiO<sub>2</sub> does not interfere the absorption of the  $\alpha$ -mangostin dye (Conformers 2) on the DSSC light conversion efficiency.

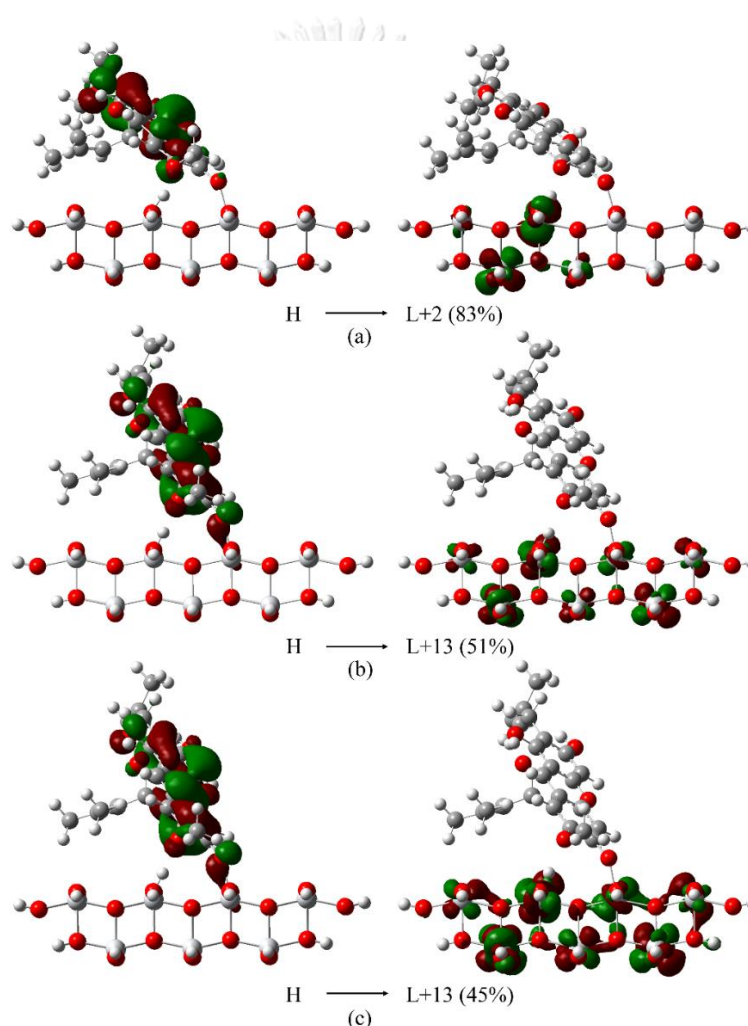


**Figure 13.** The orbitals related with major electron transitions, plotted of (a) the HOMO and LUMO+2 orbitals of the Conformers 2/TiO<sub>2</sub> in vacuo, (b) and (c) the HOMO and LUMO+13 orbitals of the Conformers 2/TiO<sub>2</sub> in acetonitrile and water, respectively.

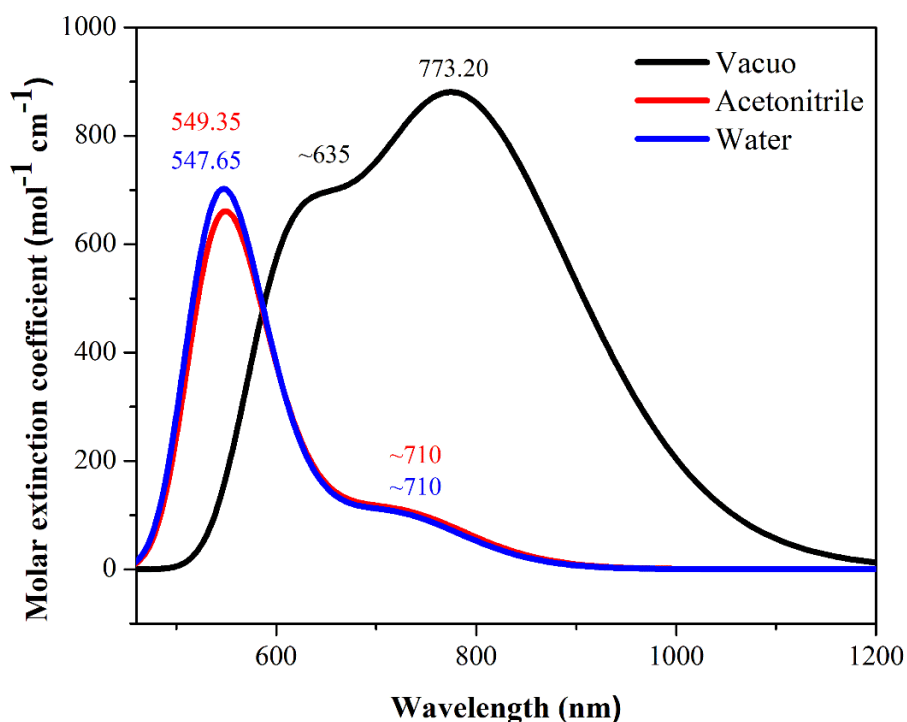


**Figure 14.** Simulated UV–Vis spectra of the of the Conformers 2/TiO<sub>2</sub> in vacuo, acetonitrile and water.

#### 4.3 Light harvesting efficiency and open circuit voltage

LHE and  $V_{oc}$  of which values in vacuo, acetonitrile and water were calculated using Eqs (2.35) and (2.37), respectively, are shown in Table 11. It shows that the LHEs of all three conformers (Conformers 2, 3 and 4) in vacuo, acetonitrile and water are within the range of 0.6757–0.7556 eV, 0.8286–0.8466 eV and 0.8288–0.8465 eV, respectively. The LHE values of three conformers in either vacuo or acetonitrile or water are in the same sequence: Conformer 2 > Conformer 4 > Conformer 3. As the solvent stabilizes the molecule compare with gas phases has been known, these conformers in solvents (acetonitrile and water) were stable than in gas phase and their LHEs were found to be larger than in the vacuo. Nevertheless, the LHE values of three conformers in acetonitrile and water are hardly different and should give similar photocurrent. The theoretical  $V_{oc}$  values of three conformers are within the range of 2.07 to 2.14 eV in vacuo and 1.96 to 1.97 eV in solvents. Nevertheless, negative

values of  $\Delta G_{\text{rec}}$  affect the theoretical  $V_{\text{OC}}$  values in terms of voltage loss. The  $\Delta G_{\text{rec}}$  values of three conformers either in vacuo or solvents are hardly different namely within the range of  $-1.98$  to  $-1.96$  eV in vacuo and  $-2.15$  to  $-2.13$  eV in solvents. As the loss due to recombination,  $V_{\text{OC}}$  values of three conformers could be less than their theoretical  $V_{\text{OC}}$  values.

**Table 11.** The open circuit voltage ( $V_{\text{OC}}$ ) and light harvesting efficiency ( $LHE$ ) of three conformers of the  $\alpha$ -mangostin in various media.

Species	Gas Phase <sup>a</sup>		Acetonitrile <sup>b</sup>		Water <sup>b</sup>	
	$V_{\text{OC}}^{\text{c}}$	$LHE^{\text{d}}$	$V_{\text{OC}}^{\text{c}}$	$LHE^{\text{d}}$	$V_{\text{OC}}^{\text{c}}$	$LHE^{\text{d}}$
Conformer 2	2.14	0.7556	1.96	0.8466	1.96	0.8465
Conformer 3	2.09	0.6757	1.97	0.8286	1.97	0.8288
Conformer 4	2.07	0.7198	1.96	0.8387	1.96	0.8387

<sup>a</sup> Based on the TD/B3LYP/6-31+G(d,p) calculations.

<sup>b</sup> Based on the TD/CPCM/UFF/B3LYP/6-31+G(d,p) calculations.

<sup>c</sup> Computed by Eq (2.37), in eV.

<sup>d</sup> Computed by Eq (2.35).

#### 4.4 Free energy of electron injection, regeneration and recombination

The ground-state energy ( $E^{\text{dye}}$ ) of three  $\alpha$ -mangostin conformers evaluated as the value of  $E_{\text{HOMO}}$  and the excited-state energy ( $E^{\text{dye*}}$ ) obtained from Eq (2.36) are shown in Table 12. The  $E^{\text{dye*}}$  values of three conformers are within the range of  $-1.24$  to  $-1.19$  eV in vacuo of which the range is broader than in solvents ( $-1.36$  to  $-1.34$  eV). The computed free energy changes of three conformers of the  $\alpha$ -mangostin are tabulated in Table 13. Negative values of all the  $\Delta G_{\text{inject}}$  and  $\Delta G_{\text{reg}}$  of  $\alpha$ -mangostin conformers in various media at 298 K, 1 atm, were found as usual thermodynamically preferred process of dye for DSSC.

The  $\Delta G_{\text{inject}}$  values of three conformers are within the range of  $-2.81$  to  $-2.76$  eV in vacuo of which the range is wider than in solvents ( $-2.66$  to  $-2.64$  eV). The  $\Delta G_{\text{reg}}$  values of three conformers are within the range of  $-1.18$  to  $-1.16$  eV in vacuo and of  $-1.35$  to  $-1.33$  eV in solvents.

**Table 12.** Values of  $E_{\lambda_{\text{max}}}$ ,  $E^{\text{dye}}$  and  $E^{\text{dye}^*}$  of three conformers of the  $\alpha$ -mangostin in various media.

Species	Gas Phase <sup>a</sup>			Acetonitrile <sup>b</sup>			Water <sup>b</sup>		
	$E_{\lambda_{\text{max}}}$ <sup>c,d</sup>	$E^{\text{dye}}$ <sup>d,e</sup>	$E^{\text{dye}^*}$ <sup>d,f</sup>	$E_{\lambda_{\text{max}}}$ <sup>c,d</sup>	$E^{\text{dye}}$ <sup>d,e</sup>	$E^{\text{dye}^*}$ <sup>d,f</sup>	$E_{\lambda_{\text{max}}}$ <sup>c,d</sup>	$E^{\text{dye}}$ <sup>d,e</sup>	$E^{\text{dye}^*}$ <sup>d,f</sup>
Conformer 2	4.77	-5.96	-1.19	4.79	-6.14	-1.36	4.79	-6.15	-1.35
Conformer 3	4.75	-5.97	-1.22	4.79	-6.13	-1.34	4.79	-6.13	-1.34
Conformer 4	4.74	-5.98	-1.24	4.78	-6.13	-1.35	4.78	-6.13	-1.35

<sup>a</sup> Based on the TD/B3LYP/6-31+G(d,p) calculations.

<sup>b</sup> Based on the TD/CPCM/UFF/B3LYP/6-31+G(d,p) calculations.

<sup>c</sup> Converted from  $\lambda_{\text{max}}$ .

<sup>d</sup> In eV.

<sup>e</sup>  $E^{\text{dye}} = -E_{\text{HOMO}}$

<sup>f</sup>  $E^{\text{dye}^*} = E_{\lambda_{\text{max}}} - E^{\text{dye}}$

**Table 13.** Terms of free energy changes of three conformers of the  $\alpha$ -mangostin in various media.

Species	Gas Phase <sup>a</sup>			Acetonitrile <sup>b</sup>			Water <sup>b</sup>		
	$\Delta G_{\text{inject}}^c$	$\Delta G_{\text{reg}}^c$	$\Delta G_{\text{rec}}^c$	$\Delta G_{\text{inject}}^c$	$\Delta G_{\text{reg}}^c$	$\Delta G_{\text{rec}}^c$	$\Delta G_{\text{inject}}^c$	$\Delta G_{\text{reg}}^c$	$\Delta G_{\text{rec}}^c$
Conformer 2	-2.81	-1.16	-1.96	-2.64	-1.34	-2.14	-2.65	-1.35	-2.15
Conformer 3	-2.78	-1.17	-1.97	-2.66	-1.33	-2.13	-2.66	-1.33	-2.13
Conformer 4	-2.76	-1.18	-1.98	-2.65	-1.33	-2.13	-2.65	-1.33	-2.13

<sup>a</sup> Based on the TD/B3LYP/6-31+G(d,p) calculations.

<sup>b</sup> Based on the TD/CPCM/UFF/B3LYP/6-31+G(d,p) calculations.

<sup>c</sup> In eV.



## CHAPTER V

### CONCLUSIONS

Five conformers of  $\alpha$ -mangostin dye (Conformers 1, 2, 3, 4 and 5) and their deprotonated and dehydrogenated species were found using different methods (DFT, periodic DFT and DFTB). The most stable conformer (Conformer 2) was considered in terms of relative energies of their deprotonated and dehydrogenated species. As reactions of the  $\alpha$ -mangostin with other substrate or material surface are considered, its Conformer 2(H3)<sup>-</sup> and Conformer 2(H3)<sup>•</sup> species are expected to be involved. The upper-rim hydroxyl group (H1O2: G2 group) was found to be the most effective group of which orientations of points its H1 toward O2 atom (G2 =  $\alpha$ ), are stable conformers (Conformers 2, 3 and 4). Therefore, three major conformers (Conformers 2, 3 and 4) were assumed to dominantly exist in the natural systems of the  $\alpha$ -mangostin.

Based on the B3LYP/6-31+G(d,p) calculations, equilibrium constants of these three conformers ( $K_{2-4}$ ,  $K_{4-3}$  and  $K_{2-3}$ ) were obtained via Gibbs free energies calculations. At 298 K and 1 atm,  $K_{2-4}$ ,  $K_{4-3}$  and  $K_{2-3}$  of ( $1.23 \times 10^{-2}$ ,  $2.91 \times 10^0$ ,  $3.58 \times 10^{-2}$ ) in vacuo, ( $1.61 \times 10^{-1}$ ,  $1.03 \times 10^0$ ,  $1.66 \times 10^{-1}$ ) in acetonitrile and ( $1.51 \times 10^{-1}$ ,  $1.03 \times 10^0$ ,  $1.56 \times 10^{-1}$ ) in water were obtained. UV-Vis absorptivities of Conformers 2, 3 and 4, in percent of (95.4%, 3.4%, 1.2%) in vacuo, (75.4%, 12.5%, 12.1%) in acetonitrile and (76.5%, 11.9%, 11.5%) in water were found. Populations of Conformers 3 and 4 were found to be more favorable in solvent phase than in gas phase. The three apparent maximum absorption wavelengths, ( $\lambda_{\max}^1$ ,  $\lambda_{\max}^2$  and  $\lambda_{\max}^3$ ) of mixtures in gas phase, acetonitrile and water were found as (259.88, 306.75 and 348.43 nm), (259.07, 311.33 and 350.63 nm) and (259.07, 311.33 and 350.63 nm), respectively. The simulated UV-Vis spectra of the Conformers 2, 3 and 4 in acetonitrile (aprotic) and water (protic solvent) were found to be good agreement with the experiments. The Conformer 2 was found to give the highest molar absorptivity in all three media.

LHEs of all three conformers (Conformers 2, 3 and 4) in vacuo, acetonitrile and water are within the range of 0.6757–0.7556 eV, 0.8286–0.8466 eV and 0.8288–0.8465 eV, respectively. The LHE values of three conformers in either vacuo or acetonitrile or water are in the same sequence: Conformer 2 > Conformer 4 > Conformer 3. The theoretical  $V_{oc}$  values of three conformers are within the range of 2.07 to 2.14 eV in vacuo and 1.96 to 1.97 eV in solvents. The light absorption of the Conformers 2/TiO<sub>2</sub> may not disturb the DSSC mechanism of the  $\alpha$ -mangostin while absorption of high energy light such at 259.88 nm in vacuo (259.07 nm and 259.07 nm in acetonitrile and water, respectively).



## REFERENCES

1. Susanti, D.; Nafi, M.; Purwaningsih, H.; Fajarin, R.; Kusuma, G. E., The Preparation of Dye Sensitized Solar Cell (DSSC) from TiO<sub>2</sub> and Tamarillo Extract. *Procedia Chemistry* **2014**, *9*, 3-10.
2. Pratik, S. M.; Datta, A., Computational Design of Concomitant Type-I and Type-II Porphyrin Sensitized Solar Cells. *Phys Chem Chem Phys* **2013**, *15*, 18471-18481.
3. Kusumawati, Y.; Massin, J.; Olivier, C.; Toupance, T.; Ivansyah, A. L.; Martoprawiro, M. A.; Prijamboedi, B.; Radiman, C. L.; Pauporté, T., Combined Computational and Experimental Study of Carbazole Dyes for Iodide- and Cobalt-Based ZnO DSSCs. *Journal of Photochemistry and Photobiology A: Chemistry* **2017**, *341*, 69-77.
4. Jeon, J.; Park, Y. C.; Han, S. S.; Goddard, W. A., 3rd; Lee, Y. S.; Kim, H., Rapid Dye Regeneration Mechanism of Dye-Sensitized Solar Cells. *J Phys Chem Lett* **2014**, *5*, 4285-4290.
5. Ye, M.; Wen, X.; Wang, M.; Iocozzia, J.; Zhang, N.; Lin, C.; Lin, Z., Recent Advances in Dye-Sensitized Solar Cells: From Photoanodes, Sensitizers and Electrolytes to Counter Electrodes. *Materials Today* **2015**, *18*, 155-162.
6. Wongcharee, K.; Meeyoo, V.; Chavadej, S., Dye-Sensitized Solar Cell Using Natural Dyes Extracted from Rosella and Blue Pea Flowers. *Solar Energy Materials and Solar Cells* **2007**, *91*, 566-571.
7. Kumara, N. T. R. N.; Lim, A.; Lim, C. M.; Petra, M. I.; Ekanayake, P., Recent Progress and Utilization of Natural Pigments in Dye Sensitized Solar Cells: A Review. *Renewable and Sustainable Energy Reviews* **2017**, *78*, 301-317.
8. Gu, P.; Yang, D.; Zhu, X.; Sun, H.; Li, J., Fabrication and Characterization of Dye-Sensitized Solar Cells Based on Natural Plants. *Chemical Physics Letters* **2018**, *693*, 16-22.
9. Ayalew, W. A.; Ayele, D. W., Dye-Sensitized Solar Cells Using Natural Dye as Light-Harvesting Materials Extracted from *Acanthus Sennii* Chiovenda Flower and *Euphorbia Cotinifolia* Leaf. *Journal of Science: Advanced Materials and Devices* **2016**, *1*, 488-494.
10. Jun, H. K.; Arof, A. K., Performance of Natural Dyes as Sensitizer in Dye-Sensitized Solar Cells Employing LiBOB-Based Liquid Electrolyte. *Ionics* **2017**, *24*, 915-922.
11. Zhou, H.; Wu, L.; Gao, Y.; Ma, T., Dye-Sensitized Solar Cells Using 20 Natural Dyes as Sensitizers. *Journal of Photochemistry and Photobiology A: Chemistry* **2011**, *219*, 188-194.
12. Tontapha, S.; Sang-aroon, W.; Kanokmedhakul, S.; Promgool, T.; Amornkitbamrung, V., Effects of Dye-Adsorption Solvents, Acidification and Dye Combination on Efficiency of DSSCs Sensitized by  $\alpha$ -Mangostin and Anthocyanin from Mangosteen Pericarp. *Journal of Materials Science: Materials in Electronics* **2017**, *28*, 7454-7467.
13. O'Regan, B.; Grätzel, M., A Low-Cost, High-Efficiency Solar Cell Based on Dye-Sensitized Colloidal TiO<sub>2</sub> Films. *Nature* **1991**, *353*, 737-740.
14. Gong, J.; Sumathy, K.; Qiao, Q.; Zhou, Z., Review on Dye-Sensitized Solar Cells (DSSCs): Advanced Techniques and Research Trends. *Renewable and Sustainable*



*Energy Reviews* **2017**, *68*, 234-246.

15. Arjunan, T. V.; Senthil, T. S., Review: Dye Sensitized Solar Cells. *Materials Technology* **2013**, *28*, 9-14.

16. Mahalingam, S.; Abdullah, H., Electron Transport Study of Indium Oxide as Photoanode in DSSCs: A Review. *Renewable and Sustainable Energy Reviews* **2016**, *63*, 245-255.

17. Hastuti, S. D.; Nurosyid, F.; Supriyanto, A.; Suryana, R., Modification of Circuit Module of Dye-Sensitized Solar Cells (DSSC) for Solar Windows Applications. *Journal of Physics: Conference Series* **2016**, 776.

18. Su'ait, M. S.; Rahman, M. Y. A.; Ahmad, A., Review on Polymer Electrolyte in Dye-Sensitized Solar Cells (DSSCs). *Solar Energy* **2015**, *115*, 452-470.

19. Marom, N.; Korzdorfer, T.; Ren, X.; Tkatchenko, A.; Chelikowsky, J. R., Size Effects in the Interface Level Alignment of Dye-Sensitized TiO<sub>2</sub> Clusters. *J Phys Chem Lett* **2014**, *5*, 2395-2401.

20. Asaduzzaman, A. M.; Schreckenbach, G., Computational Studies on the Interactions among Redox Couples, Additives and TiO<sub>2</sub>: Implications for Dye-Sensitized Solar Cells. *Phys Chem Chem Phys* **2010**, *12*, 14609-14618.

21. Li, M.; Kou, L.; Diao, L.; Zhang, Q.; Li, Z.; Wu, Q.; Lu, W.; Pan, D., Theoretical Study of Acene-Bridged Dyes for Dye-Sensitized Solar Cells. *J Phys Chem A* **2015**, *119*, 3299-3309.

22. Areerob, Y.; Cho, K.-Y.; Oh, W.-C., Strategy to Improve Photovoltaic Performance of DSSC Sensitized by Using Novel Nanostructured La Doped TiO<sub>2</sub>-Graphene Electrodes. *Journal of Materials Science: Materials in Electronics* **2017**, *29*, 3437-3448.

23. Lee, C.-P.; Li, C.-T.; Ho, K.-C., Use of Organic Materials in Dye-Sensitized Solar Cells. *Materials Today* **2017**, *20*, 267-283.

24. Zhang, J.; Zhou, P.; Liu, J.; Yu, J., New Understanding of the Difference of Photocatalytic Activity among Anatase, Rutile and Brookite TiO<sub>2</sub>. *Phys Chem Chem Phys* **2014**, *16*, 20382-20386.

25. Chen, W.; Kuang, Q.; Wang, Q.; Xie, Z., Engineering a High Energy Surface of Anatase TiO<sub>2</sub> Crystals Towards Enhanced Performance for Energy Conversion and Environmental Applications. *RSC Advances* **2015**, *5*, 20396-20409.

26. Zhang, M.; Chen, T.; Wang, Y., Insights into TiO<sub>2</sub> Polymorphs: Highly Selective Synthesis, Phase Transition, and Their Polymorph-Dependent Properties. *RSC Advances* **2017**, *7*, 52755-52761.

27. Haggerty, J. E. S., et al., High-Fraction Brookite Films from Amorphous Precursors. *Sci Rep* **2017**, *7*, 15232.

28. Diebold, U., The Structure of TiO<sub>2</sub> Surfaces. In *Oxide Surfaces*, 2001, 443-484.

29. Tsega, M.; Dejene, F. B., Influence of Acidic PH on the Formulation of TiO<sub>2</sub> Nanocrystalline Powders with Enhanced Photoluminescence Property. *Heliyon* **2017**, *3*, 246.

30. Hanaor, D. A. H.; Sorrell, C. C., Review of the Anatase to Rutile Phase Transformation. *Journal of Materials Science* **2010**, *46*, 855-874.

31. Arias, L. M. F.; Duran, A. A.; Cardona, D.; Camps, E.; Gómez, M. E.; Zambrano, G., Effect of Annealing Treatment on the Photocatalytic Activity of TiO<sub>2</sub> thin Films Deposited by Dc Reactive Magnetron Sputtering. *Journal of Physics: Conference Series* **2015**, 614.

32. Kashiwaya, S.; Morasch, J.; Streibel, V.; Toupance, T.; Jaegermann, W.; Klein, A., *The Work Function of TiO<sub>2</sub>* **2018**, *1*, 73-89.
33. Howard, C. J.; Sabine, T. M.; Dickson, F., Structural and Thermal Parameters for Rutile and Anatase. *Acta Crystallographica Section B* **1991**, *47*, 462-468.
34. Zhang, H.; Banfield, J. F., Thermodynamic Analysis of Phase Stability of Nanocrystalline Titania. *Journal of Materials Chemistry* **1998**, *8*, 2073-2076.
35. Cheng, X.; Li, F.; Zhao, Y., A Dft Investigation on ZnO Clusters and Nanostructures. *Journal of Molecular Structure: THEOCHEM* **2009**, *894*, 121-127.
36. Diebold, U., The Surface Science of Titanium Dioxide. *Surface Science Reports* **2003**, *48*, 53-229.
37. Zou, W.; Feng, R.; Yang, Y., Changes in the Serum Levels of Inflammatory Cytokines in Antidepressant Drug-Naive Patients with Major Depression. *PLoS One* **2018**, *13*, 197.
38. Nava Catorce, M.; Acero, G.; Pedraza-Chaverri, J.; Fragoso, G.; Govezensky, T.; Gevorkian, G., Alpha-Mangostin Attenuates Brain Inflammation Induced by Peripheral Lipopolysaccharide Administration in C57BL/6j Mice. *J Neuroimmunol* **2016**, *297*, 20-27.
39. Won, Y. S.; Lee, J. H.; Kwon, S. J.; Kim, J. Y.; Park, K. H.; Lee, M. K.; Seo, K. I., Alpha-Mangostin-Induced Apoptosis Is Mediated by Estrogen Receptor Alpha in Human Breast Cancer Cells. *Food Chem Toxicol* **2014**, *66*, 158-165.
40. Mohan, S.; Syam, S.; Abdelwahab, S. I.; Thangavel, N., An Anti-Inflammatory Molecular Mechanism of Action of Alpha-Mangostin, the Major Xanthone from the Pericarp of Garcinia Mangostana: An in Silico, in Vitro and in Vivo Approach. *Food Funct* **2018**, *9*, 3860-3871.
41. Guzman-Beltran, S.; Rubio-Badillo, M. A.; Juarez, E.; Hernandez-Sanchez, F.; Torres, M., Nordihydroguaiaretic Acid (NDGA) and Alpha-Mangostin Inhibit the Growth of Mycobacterium Tuberculosis by Inducing Autophagy. *Int Immunopharmacol* **2016**, *31*, 149-157.
42. Phuong, N. T. M.; Van Quang, N.; Mai, T. T.; Anh, N. V.; Kuhakarn, C.; Reutrakul, V.; Bolhuis, A., Antibiofilm Activity of Alpha-Mangostin Extracted from Garcinia Mangostana L. Against Staphylococcus Aureus. *Asian Pac J Trop Med* **2017**, *10*, 1154-1160.
43. Guo, Y.; Deng, Y.; Li, X.; Ning, Y.; Lin, X.; Guo, S.; Chen, M.; Han, M., Glutaminolysis Was Induced by TGF-Beta1 through PP2AC Regulated Raf-MEK-ERK Signaling in Endothelial Cells. *PLoS One* **2016**, *11*, 162.
44. Wudtiwai, B.; Pitchakarn, P.; Banjerdpongchai, R., Alpha-Mangostin, an Active Compound in Garcinia Mangostana, Abrogates Anoikis-Resistance in Human Hepatocellular Carcinoma Cells. *Toxicol In Vitro* **2018**, *53*, 222-232.
45. Chen, G.; Li, Y.; Wang, W.; Deng, L., Bioactivity and Pharmacological Properties of Alpha-Mangostin from the Mangosteen Fruit: A Review. *Expert Opin Ther Pat* **2018**, *28*, 415-427.
46. Jaisin, Y.; Ratanachamnong, P.; Kuanpradit, C.; Khumpum, W.; Suksamrarn, S., Protective Effects of Gamma-Mangostin on 6-OHDA-Induced Toxicity in SH-SY5Y Cells. *Neurosci Lett* **2018**, *665*, 229-235.
47. Tarasuk, M.; Songprakhon, P.; Chamma, P.; Sratongno, P.; Na-Bangchang, K.; Yenchitsomanus, P. T., Alpha-Mangostin Inhibits Both Dengue Virus Production and Cytokine/Chemokine Expression. *Virus Res* **2017**, *240*, 180-189.

48. Thiel, W., *Semiempirical Quantum–Chemical Methods*. *Wiley Interdisciplinary Reviews: Computational Molecular Science* **2013**, *4*, 145-157.
49. Xu, J. M.; Huang, P. M., *Molecular Environmental Soil Science at the Interfaces in the Earth's Critical Zone*; Springer Berlin Heidelberg **2011**.
50. Young, D., *Computational Chemistry: A Practical Guide for Applying Techniques to Real World Problems*; Wiley **2004**.
51. Lewars, E., *Computational Chemistry: Introduction to the Theory and Applications of Molecular and Quantum Mechanics*; Springer **2003**.
52. Eschrig, H., *The Fundamentals of Density Functional Theory*; Vieweg+Teubner Verlag **2012**.
53. Parr, R. G.; Yang, W., *Density-Functional Theory of Atoms and Molecules*; Oxford University Press, USA **1994**.
54. Misra, P. K., Metallic Nanoclusters. In *Physics of Condensed Matter* **2012**, 527-566.
55. Mortimer, R. G., *Physical Chemistry*; Elsevier Science **2008**.
56. Evarestov, R. A., *Theoretical Modeling of Inorganic Nanostructures: Symmetry and Ab-Initio Calculations of Nanolayers, Nanotubes and Nanowires*; Springer Berlin Heidelberg **2015**.
57. Anslyn, E. V.; Dougherty, D. A.; Dougherty, E. V.; Books, U. S., *Modern Physical Organic Chemistry*; University Science Books **2006**.
58. Magalhães, A. L., Gaussian-Type Orbitals Versus Slater-Type Orbitals: A Comparison. *Journal of Chemical Education* **2014**, *91*, 2124-2127.
59. Szabo, A.; Ostlund, N. S., *Modern Quantum Chemistry: Introduction to Advanced Electronic Structure Theory*; Dover Publications **1996**.
60. McDouall, J. J. W., *Computational Quantum Chemistry: Molecular Structure and Properties in Silico*; RSC Publishing **2013**.
61. Evarestov, R. A., *Quantum Chemistry of Solids: The LCAO First Principles Treatment of Crystals*; Springer Berlin Heidelberg **2007**.
62. Bachrach, S. M., *Computational Organic Chemistry*; Wiley **2007**.
63. Jensen, F., *Introduction to Computational Chemistry*; Wiley **2016**.
64. Baia, M.; Astilean, S.; Iliescu, T., *Raman and Sers Investigations of Pharmaceuticals*; Springer Berlin Heidelberg **2008**.
65. Elstner, M.; Seifert, G., Density Functional Tight Binding. *Philos Trans A Math Phys Eng Sci* **2014**, *372*, 20120483.
66. Elstner, M., The SCC-DFTB Method and Its Application to Biological Systems. *Theoretical Chemistry Accounts* **2005**, *116*, 316-325.
67. Ardo, S.; Meyer, G. J., Photodriven Heterogeneous Charge Transfer with Transition-Metal Compounds Anchored to TiO<sub>2</sub> Semiconductor Surfaces. *Chem Soc Rev* **2009**, *38*, 115-164.
68. Narayan, M. R., Review: Dye Sensitized Solar Cells Based on Natural Photosensitizers. *Renewable and Sustainable Energy Reviews* **2011**.
69. Zhang, J.; Li, H.-B.; Zhang, J.-Z.; Wu, Y.; Geng, Y.; Fu, Q.; Su, Z.-M., A Promising Anchor Group for Efficient Organic Dye Sensitized Solar Cells with Iodine-Free Redox Shuttles: A Theoretical Evaluation. *Journal of Materials Chemistry A* **2013**, *1*.
70. Zhang, J.; Li, H.-B.; Sun, S.-L.; Geng, Y.; Wu, Y.; Su, Z.-M., Density Functional Theory Characterization and Design of High-Performance Diarylamine-

Fluorenydyes with Different  $\Pi$  Spacers for Dye-Sensitized Solar Cells. *J. Mater. Chem.* **2012**, *22*, 568-576.

71. Feng, J.; Jiao, Y.; Ma, W.; Nazeeruddin, M. K.; Grätzel, M.; Meng, S., First Principles Design of Dye Molecules with Ullazine Donor for Dye Sensitized Solar Cells. *The Journal of Physical Chemistry C* **2013**, *117*, 3772-3778.

72. Lu, X.; Wei, S.; Wu, C.-M. L.; Li, S.; Guo, W., Can Polypyridyl Cu(I)-Based Complexes Provide Promising Sensitizers for Dye-Sensitized Solar Cells? A Theoretical Insight into Cu(I) Versus Ru(II) Sensitizers. *The Journal of Physical Chemistry C* **2011**, *115*, 3753-3761.

73. Zhang, J.; Kan, Y.-H.; Li, H.-B.; Geng, Y.; Wu, Y.; Su, Z.-M., How to Design Proper  $\pi$ -Spacer Order of the D- $\pi$ -a Dyes for DSSCs? A Density Functional Response. *Dyes and Pigments* **2012**, *95*, 313-321.

74. Katoh, R.; Furube, A.; Yoshihara, T.; Hara, K.; Fujihashi, G.; Takano, S.; Murata, S.; Arakawa, H.; Tachiya, M., Efficiencies of Electron Injection from Excited N3 Dye into Nanocrystalline Semiconductor (ZrO<sub>2</sub>, TiO<sub>2</sub>, ZnO, Nb<sub>2</sub>O<sub>5</sub>, SnO<sub>2</sub>, In<sub>2</sub>O<sub>3</sub>) Films. *Journal of Physical Chemistry B* **2004**, *108*, 4818-4822.

75. El-Meligy, A. B.; Koga, N.; Iuchi, S.; Yoshida, K.; Hirao, K.; Mangood, A. H.; El-Nahas, A. M., DFT/TD-DFT Calculations of the Electronic and Optical Properties of Bis-N,N-Dimethylaniline-Based Dyes for Use in Dye-Sensitized Solar Cells. *Journal of Photochemistry and Photobiology A: Chemistry* **2018**, *367*, 332-346.

76. Grätzel, M., Photoelectrochemical Cells. *Nature* **2001**, *414*, 338-344.

77. Odobel, F.; Le Pleux, L.; Pellegrin, Y.; Blart, E., New Photovoltaic Devices Based on the Sensitization of P-Type Semiconductors: Challenges and Opportunities. *Accounts of Chemical Research* **2010**, *43*, 1063-1071.

78. Cahen, D.; Hodes, G.; Grätzel, M.; Guillemoles, J. F.; Riess, I., Nature of Photovoltaic Action in Dye-Sensitized Solar Cells. *Journal of Physical Chemistry B* **2000**, *104*, 2053-2059.

79. Becke, A. D., Density-Functional Thermochemistry. III. The Role of Exact Exchange. *The Journal of Chemical Physics* **1993**, *98*, 5648-5652.

80. Lee, C.; Yang, W.; Parr, R. G., Development of the Colle-Salvetti Correlation-Energy Formula into a Functional of the Electron Density. *Physical Review B* **1988**, *37*, 785-789.

81. Hehre, W. J.; Ditchfield, K.; Pople, J. A., Self-Consistent Molecular Orbital Methods. Xii. Further Extensions of Gaussian-Type Basis Sets for Use in Molecular Orbital Studies of Organic Molecules. *The Journal of Chemical Physics* **1972**, *56*, 2257-2261.

82. Ditchfield, R.; Hehre, W. J.; Pople, J. A., Self-Consistent Molecular-Orbital Methods. IX. An Extended Gaussian-Type Basis for Molecular-Orbital Studies of Organic Molecules. *The Journal of Chemical Physics* **1971**, *54*, 720-723.

83. Frisch, M. J. T., G. W.; Schlegel, H. B.; Scuseria, G. E.; Robb, M. A.; Cheeseman, J. R.; et al., *Gaussian 09 Revision D.01*, Gaussian Inc., Wallingford, Ct, **2014**.

84. Cancès, E.; Mennucci, B.; Tomasi, J., A New Integral Equation Formalism for the Polarizable Continuum Model: Theoretical Background and Applications to Isotropic and Anisotropic Dielectrics. *The Journal of Chemical Physics* **1997**, *107*, 3032-3041.

85. Tomasi, J.; Mennucci, B.; Cammi, R., Quantum Mechanical Continuum

Solvation Models. *Chemical Reviews* **2005**, *105*, 2999-3093.

86. Tomasi, J.; Persico, M., Molecular Interactions in Solution: An Overview of Methods Based on Continuous Distributions of the Solvent. *Chemical Reviews* **1994**, *94*, 2027-2094.

87. Barone, V.; Cossi, M., Quantum Calculation of Molecular Energies and Energy Gradients in Solution by a Conductor Solvent Model. *Journal of Physical Chemistry A* **1998**, *102*, 1995-2001.

88. Cossi, M.; Barone, V., Analytical Second Derivatives of the Free Energy in Solution by Polarizable Continuum Models. *Journal of Chemical Physics* **1998**, *109*, 6246-6254.

89. Cossi, M.; Rega, N.; Scalmani, G.; Barone, V., Energies, Structures, and Electronic Properties of Molecules in Solution with the C-PCM Solvation Model. *Journal of Computational Chemistry* **2003**, *24*, 669-681.

90. Rappé, A. K.; Casewit, C. J.; Colwell, K. S.; Goddard, W. A.; Skiff, W. M., Uff, a Full Periodic Table Force Field for Molecular Mechanics and Molecular Dynamics Simulations. *Journal of the American Chemical Society* **1992**, *114*, 10024-10035.

91. Adamo, C.; Jacquemin, D., The Calculations of Excited-State Properties with Time-Dependent Density Functional Theory. *Chemical Society Reviews* **2013**, *42*, 845-856.

92. Laurent, A. D.; Adamo, C.; Jacquemin, D., Dye Chemistry with Time-Dependent Density Functional Theory. *Physical Chemistry Chemical Physics* **2014**, *16*, 14334-14356.

93. Varetto, U., Molekel 5.4. 0.8. *Swiss National Supercomputing Centre, Manno, Switzerland* **2009**.

94. Gatti, C.; Saunders, V. R.; Roetti, C., Crystal Field Effects on the Topological Properties of the Electron Density in Molecular Crystals: The Case of Urea. *The Journal of Chemical Physics* **1994**, *101*, 10686-10696.

95. Catti, M.; Pavese, A.; Dovesi, R.; Saunders, V. R., Static Lattice and Electron Properties of MgCO<sub>3</sub> (Magnesite) Calculated by Ab Initio Periodic Hartree-Fock Methods. *Physical Review B* **1993**, *47*, 9189-9198.

96. Bredow, T.; Jug, K.; Evarestov, R. A., Electronic and Magnetic Structure of ScMnO<sub>3</sub>. *physica status solidi (b)* **2006**, *243*, 10-12.

97. Aradi, B.; Hourahine, B.; Frauenheim, T., DFTB+, a Sparse Matrix-Based Implementation of the DFTB Method. *Journal of Physical Chemistry A* **2007**, *111*, 5678-5684.

98. O'boyle, N. M.; Tenderholt, A. L.; Langner, K. M., CcLib: A Library for Package-Independent Computational Chemistry Algorithms. *Journal of computational chemistry* **2008**, *29*, 839-845.

## VITA

<b>NAME</b>	Kanthira Kaewsud	
<b>DATE OF BIRTH</b>	6 July 1994	
<b>PLACE OF BIRTH</b>	Khon Kaen, Thailand	
<b>INSTITUTIONS ATTENDED</b>	2017-2019	M.Sc. (Chemistry), Chulalongkorn University, Thailand
	2013-2016	B.Sc. (Chemistry), Khon Kaen University, Thailand
	2007-2012	The Demonstration School Khon Kaen University (Modindaeng), Thailand
	2001-2006	The Demonstration School Khon Kaen University (Modindaeng), Thailand

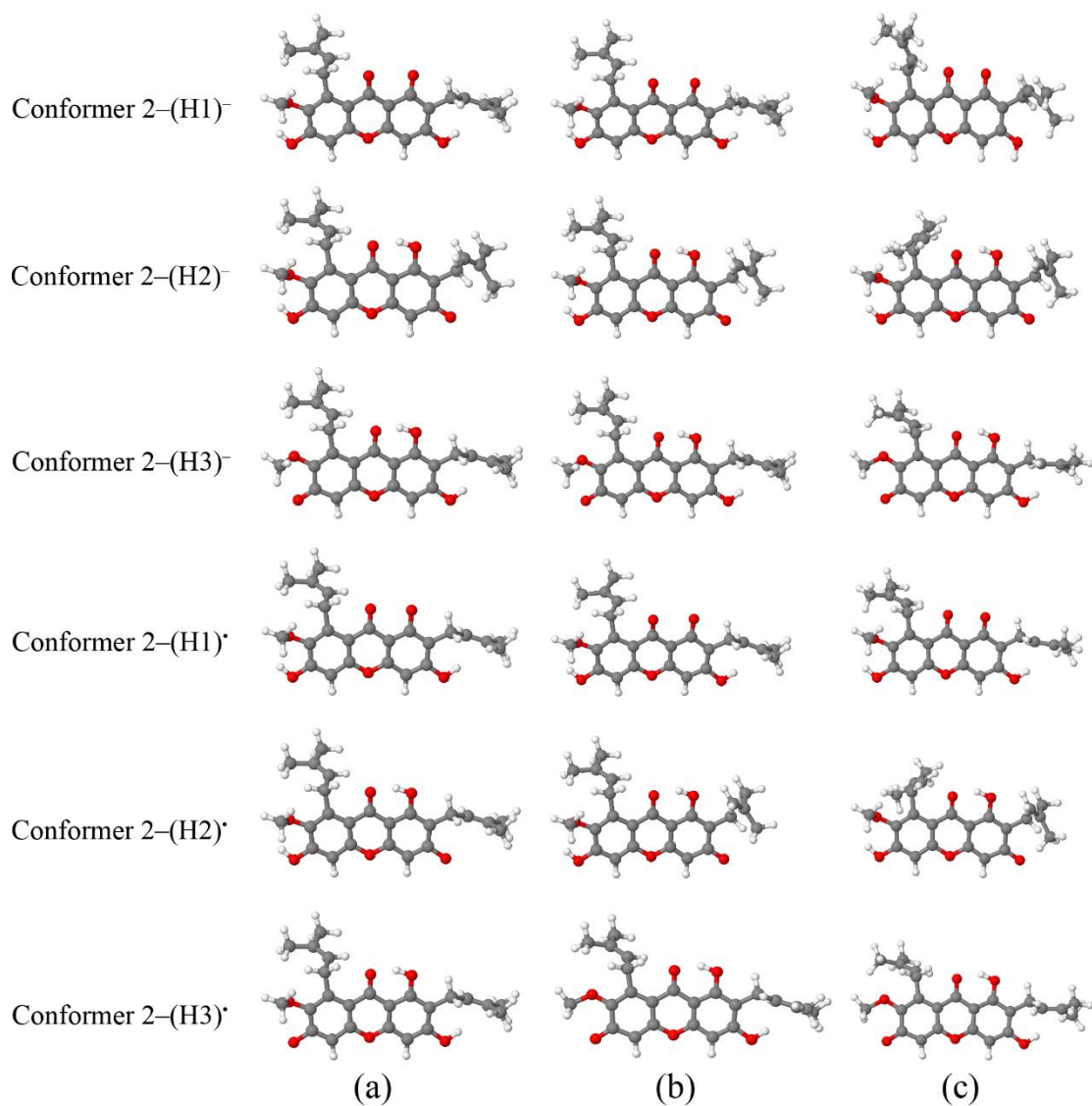


จุฬาลงกรณ์มหาวิทยาลัย  
CHULALONGKORN UNIVERSITY



**APPENDICES**

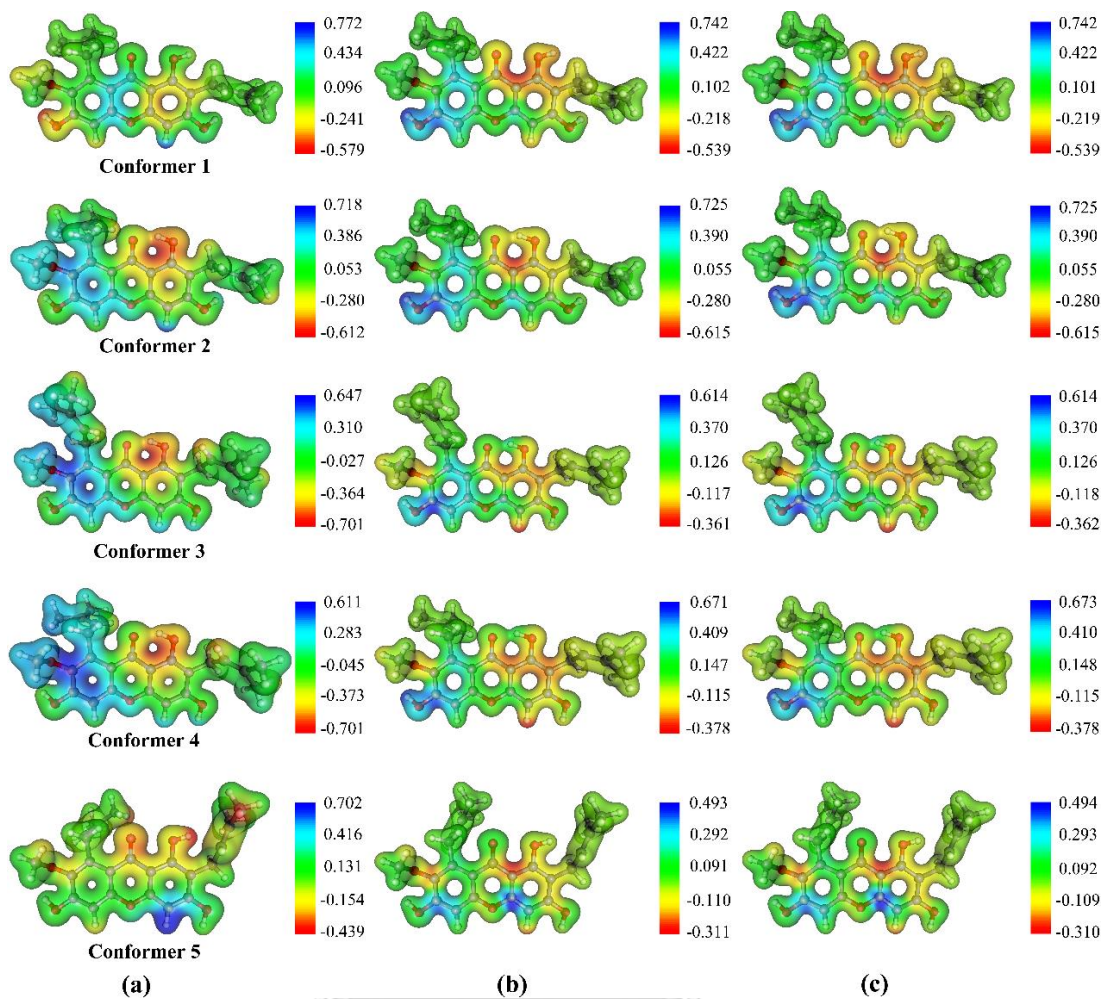
จุฬาลงกรณ์มหาวิทยาลัย  
**CHULALONGKORN UNIVERSITY**



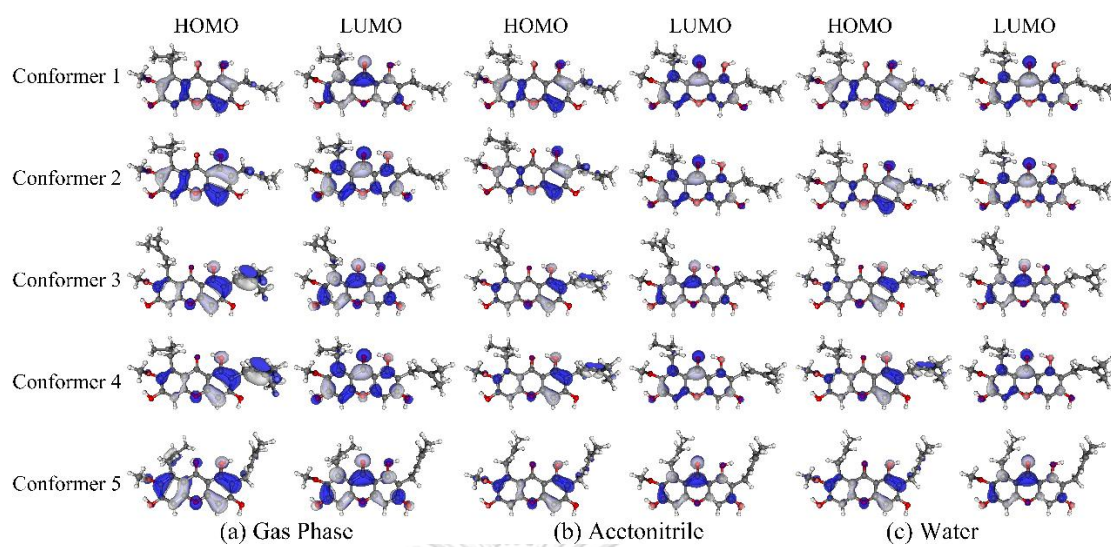
CHULALONGKORN UNIVERSITY

**Figure A-1.** Optimized structures of deprotonated ( $\text{LO}^-$ ) and dehydrogenated ( $\text{LO}^\bullet$ ) species of conformer in gas phase obtained by (a) B3LYP/6-31+G(d,p), (b) periodic DFT and (c) periodic DFTB computations.

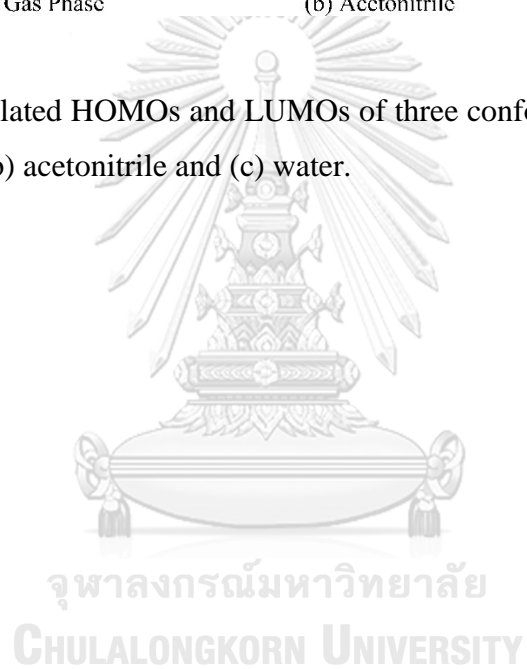


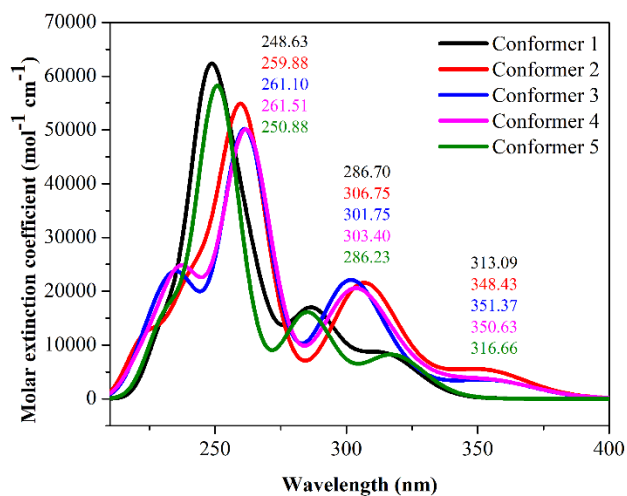


**Figure A–2.** Electrostatic potential maps with iso–surface value of  $0.03 \text{ e} \text{ \AA}^{-3}$ , showing charge density distribution of five conformers of the  $\alpha$ –mangostin in (a) gas phase, (b) acetonitrile and (c) water, based on their B3LYP/6–31+G(d,p)–optimized structures.

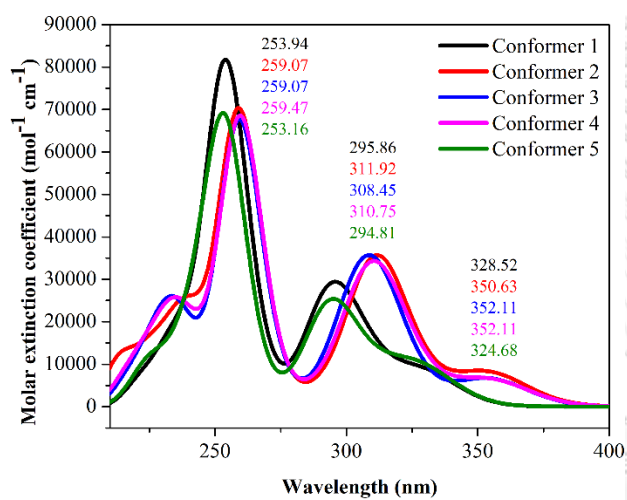


**Figure A-3.** Simulated HOMOs and LUMOs of three conformers of the  $\alpha$ -mangostin in (a) gas phase, (b) acetonitrile and (c) water.

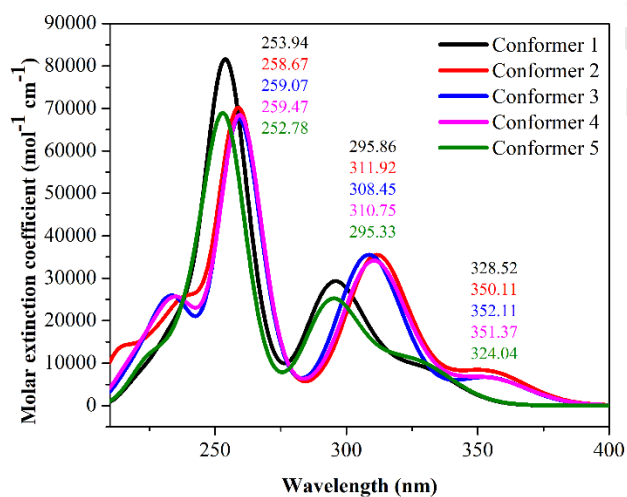




(a)



(b)



(c)

**Figure A-4.** The simulated UV/Vis absorption spectra of five conformers of  $\alpha$ -mangostin conformers in (a) gas phase, (b) acetonitrile and (c) water, based on their corresponding TD/B3LYP/6-31+G(d,p) calculations.

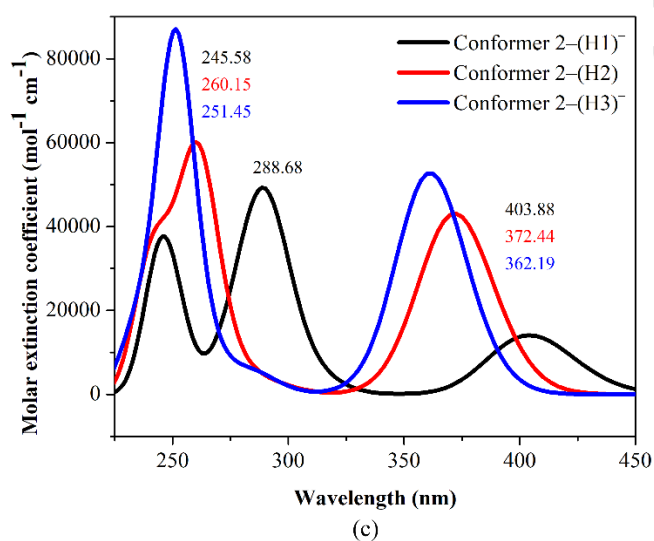
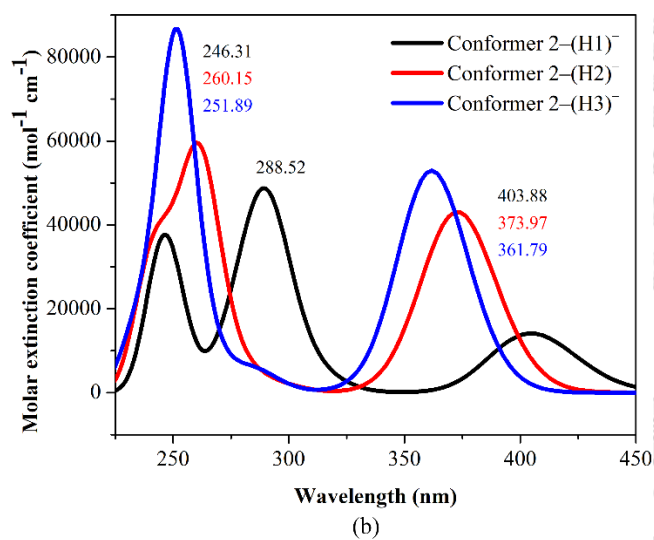
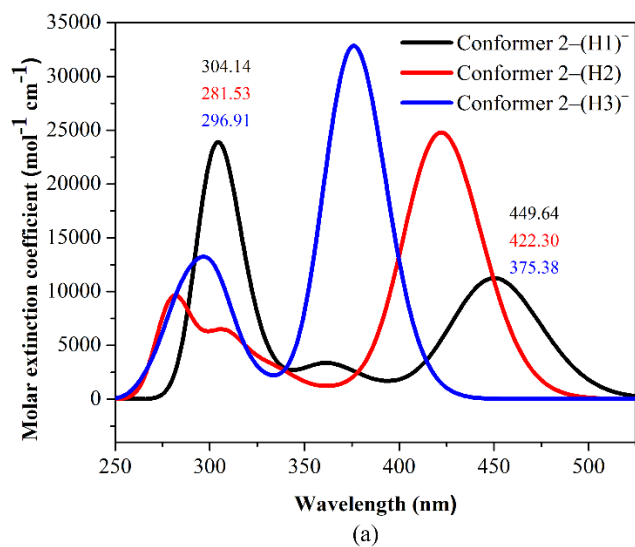


**Figure A-5.** Simulated UV-Vis spectra of deprotonated species of conformer 2 of  $\alpha$ -mangostin in (a) gas phase, (b) acetonitrile and (c) water.

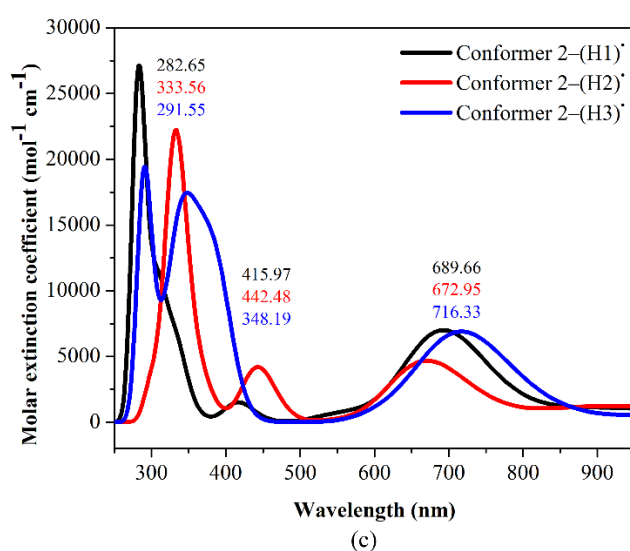
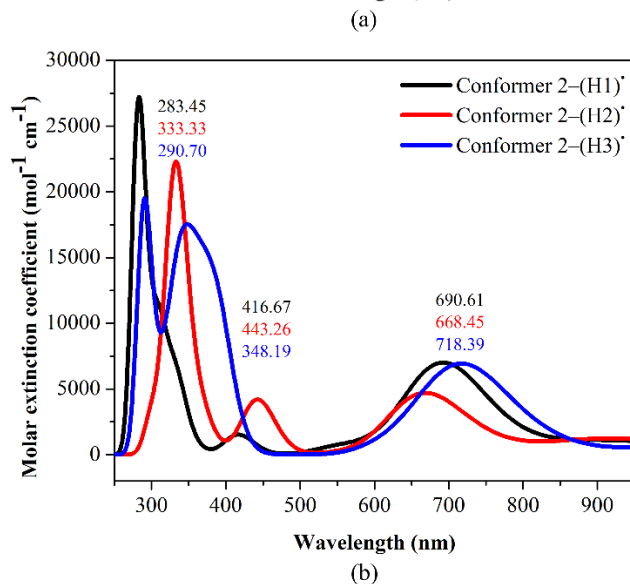
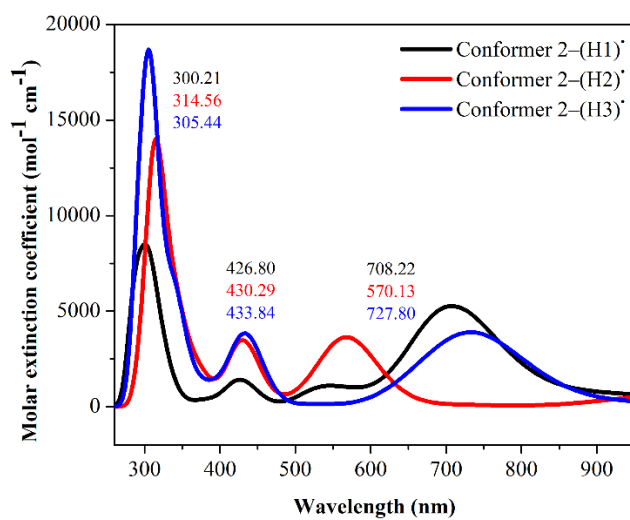


**Figure A-6.** Simulated UV-Vis spectra of dehydrogenated species of conformer 2 of  $\alpha$ -mangostin in (a) gas phase, (b) acetonitrile and (c) water.

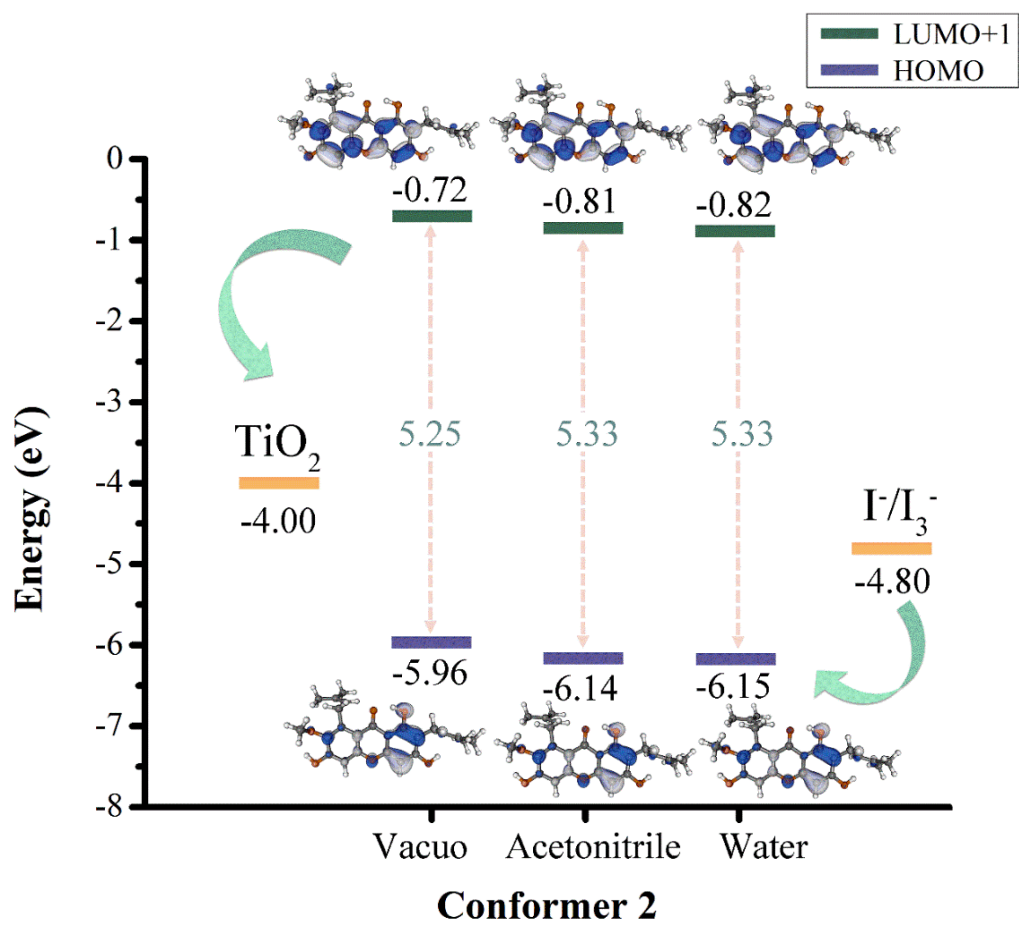


**Figure A-7.** HOMOs and LUMOs of conformer 2 of the  $\alpha$ -mangostin in (a) vacuo, (b) acetonitrile and (c) water calculated with B3LYP/6-31+G(d,p) method.



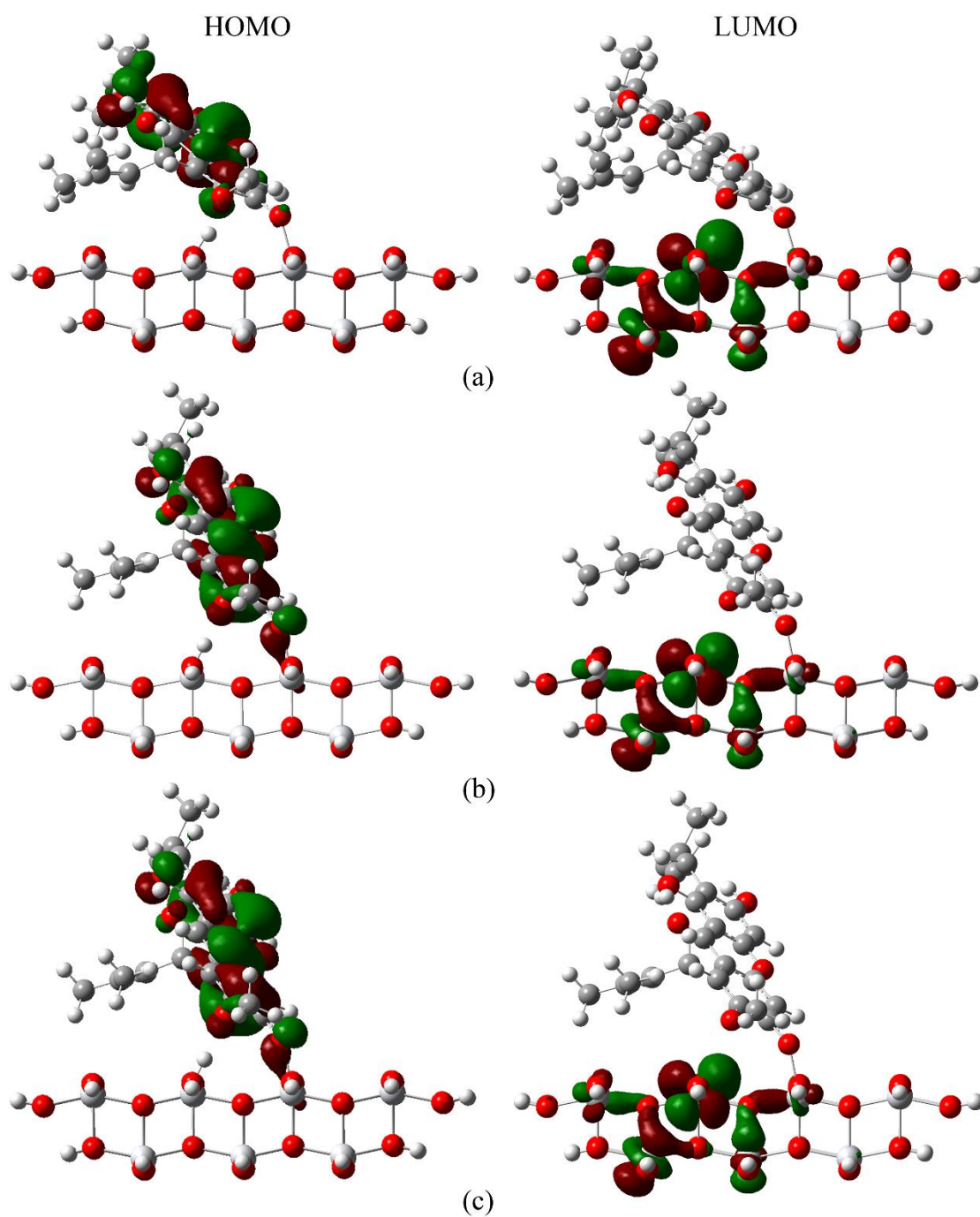


**Figure A-8.** Simulated HOMOs and LUMOs of Conformer 2/TiO<sub>2</sub> (001) surface in (a) vacuo, (b) acetonitrile and (c) water.